Signatures of antagonistic pleiotropy in a bacterial flagellin epitope

Katarzyna Parys,[1,9,8] Nicholas R. Colaianni,[2,3,8] Ho-Seok Lee,[1,8] Ulrich Hohmann,[4,10,11] Natalie Edelbacher,[1] Alen Trgovcevic,[1] Zuzana Blahovska,[1] Duhwa Lee,[1] Alexander Mechtler,[1] Zsuzsanna Muhari-Portik,[1] Mathias Madalinski,[1] Niklas Schandry,[1,9] Isaac Rodríguez-Arévalo,[1,9] Claude Becker,[1,9] Elisabeth Sonnleitner,[5] Arthur Korte,[6] Udo Bläsi,[5] Niko Geldner,[7] Michael Hothorn,[4] Corbin D. Jones,[3,*] Jeffery L. Dangl,[2,*] and Youssef Belkhadir[1,12,*]

[1]Gregor Mendel Institute (GMI), Austrian Academy of Sciences, Vienna BioCenter (VBC), Dr. Bohr-Gasse 3, Vienna, Austria
[2]Department of Biology and Howard Hughes Medical Institute, University of North Carolina at Chapel Hill, Chapel Hill, NC, USA
[3]Department of Biology, Curriculum in Bioinformatics and Computational Biology, University of North Carolina at Chapel Hill, Chapel Hill, NC, USA
[4]Structural Plant Biology Laboratory, Department of Botany and Plant Biology, University of Geneva, 1211 Geneva, Switzerland
[5]Department of Microbiology, Immunobiology and Genetics, Max Perutz Laboratories, Center of Molecular Biology, University of Vienna, Vienna Biocenter (VBC), Dr. Bohr Gasse 9, Vienna, Austria
[6]Center for Computational and Theoretical Biology, University of Würzburg, Würzburg, Germany
[7]Department of Plant Molecular Biology, University of Lausanne, Lausanne, Switzerland
[8]These authors contributed equally
[9]Present address: Faculty of Biology, Genetics, University of Munich (LMU), 82152 Martinsried, Germany
[10]Present address: IMBA - Institute of Molecular Biotechnology (IMBA), Vienna Biocenter (VBC), Dr Bohr Gasse 3, Vienna, Austria
[11]Present address: IMP - Institute of Molecular Pathology, Vienna Biocenter (VBC), Campus-Vienna, Biocenter 1, 1030 Vienna, Austria
[12]Lead contact
*Correspondence: cdjones@email.unc.edu (C.D.J.), dangl@email.unc.edu (J.L.D.), youssef.belkhadir@gmi.oeaw.ac.at (Y.B.)
https://doi.org/10.1016/j.chom.2021.02.008

SUMMARY

Immune systems respond to "non-self" molecules termed microbe-associated molecular patterns (MAMPs). Microbial genes encoding MAMPs have adaptive functions and are thus evolutionarily conserved. In the presence of a host, these genes are maladaptive and drive antagonistic pleiotropy (AP) because they promote microbe elimination by activating immune responses. The role AP plays in balancing the functionality of MAMP-coding genes against their immunogenicity is unknown. To address this, we focused on an epitope of flagellin that triggers antibacterial immunity in plants. Flagellin is conserved because it enables motility. Here, we decode the immunogenic and motility profiles of this flagellin epitope and determine the spectrum of amino acid mutations that drives AP. We discover two synthetic mutational tracks that undermine the detection activities of a plant flagellin receptor. These tracks generate epitopes with either antagonist or weaker agonist activities. Finally, we find signatures of these tracks layered atop each other in natural *Pseudomonads*.

INTRODUCTION

Innate immune systems of both plants and animals have evolved to promote the elimination of invading microbes by detecting and responding to "non-self" molecules such as microbe-associated molecular patterns (MAMPs) (Dangl et al., 2013; Iwasaki and Medzhitov, 2015). Microbial genes encoding proteinaceous MAMPs are evolutionarily conserved, broadly distributed, and indispensable for core organismal functions (McCann et al., 2012; Mott et al., 2016). Thus, when facing the activities of a host immune system, the function of these genes mediates opposed effects on microbial fitness, a concept known as antagonistic pleiotropy (AP) (Chen and Zhang, 2020). AP arises when the negative pressure to maintain vital MAMP-coding protein function is opposed to a positive pressure acting to mediate evasion from immune system detection. AP counteracts natural selection by maintaining allele variation in population despite the availability of beneficial mutations (Venkataram et al., 2020). Yet, its effect on the functionality of MAMP-coding genes is rarely, if ever, investigated.

To address this, we focused on flagellin, the main structural component of the bacterial flagellum (Macnab, 2003; Yonekura et al., 2003). The flagellin gene *fliC* is conserved and under strong evolutionary pressure because it plays an essential role in enabling bacterial motility (Ramos et al., 2004). Flagellar-based motility is essential for the maximal virulence of several human and plant pathogens (Rossez et al., 2015). In a classic case of evolutionary convergence, metazoans and plants have

independently evolved sensors that detect flagellin as a MAMP (Fliegmann and Felix, 2016). In mammals, Toll-like receptor 5 (TLR5) detect flagellin outside cells (Iwasaki and Medzhitov, 2004). Distinguishing organizational principles of the plant flagellin signaling pathways are: (1) plants perceive flagellin at the cell surface using the membrane-bound receptors FLAGELLIN SENSING 2 and 3 (FLS2 and FLS3) (Hind et al., 2016), (2) plant flagellin sensors detect, and are activated by, short peptide epitopes that are likely derived from degradation products of flagellin, as opposed to TLR5 which senses an entire domain concealed in a folded flagellin molecule (Buscaill et al., 2019; Sun et al., 2013; Yoon et al., 2012), and (3) the key signaling output, MAMP-triggered immunity, provides a rapid and broad-spectrum immune response (Hacquard et al., 2017; Lee and Belkhadir, 2020; Teixeira et al., 2019). With short microbial epitopes that physically interface with host immune receptors, the molecular mechanisms of flagellin sensing in plants provide an outstanding system to study the molecular footprints of AP.

In *Arabidopsis thaliana* (hereafter Arabidopsis), the reference plant system of this study, a 22-amino-acid epitope peptide derived from the N terminus of flagellin (flg22) is sufficient to activate FLS2 signaling (Chinchilla et al., 2006; Felix et al., 1999; Gómez-Gómez and Boller, 2000). Arabidopsis mutant plants lacking *FLS2* function are more susceptible to infection by bacterial pathogens such as *Pseudomonas syringae* (*P. syringae* or *Ps*) (Zipfel et al., 2004). In general, the genus Pseudomonas comprises a wide range of behaviorally different species that can colonize humans and/or plants (Sitaraman, 2015), and *Pseudomonads* are commonly found in the leaf microbiome of Arabidopsis (Bodenhausen et al., 2013; Chen et al., 2020; Delmotte et al., 2009; Karasov et al., 2018). flg22 is extremely well conserved in Pseudomonas pathovars, and epitope conservation is paramount for *Pseudomonas aeruginosa* (hereafter *Pa*). Despite this extreme conservation, a few individual amino acids are polymorphic, providing some diversity in the epitope. These variations may represent bacterial attempts to evolve undetectable flg22 epitopes to avoid host recognition while remaining motile (Clarke et al., 2013). The function of flg22 on bacterial motility has been addressed in studies involving a very narrow set of mutations targeting only a couple of residues (Naito et al., 2008; Wang et al., 2015). As a consequence, we still do not understand how the evolutionary trap mediated by FLS2 drives AP, and how, in turn, this has led to the conservation or diversification of some residues in flg22.

Here, we address this knowledge gap by merging synthetic biology and directed evolution into a single approach. We used the flg22 peptide from *Pa* (Pa flg22) as a reference peptide, since its interaction with the extracellular domain of FLS2 is understood at the atomic level (Sun et al., 2013), and the molecular responses it induces are the most characterized (Chinchilla et al., 2007; Schulze et al., 2010). The central goal of this study was to deconstruct both the immunogenic and motility profile of Pa flg22 by deep mutational scans to determine the spectrum of amino acids in the epitope that induce AP. First, we determined the landscape of mutational impacts on motility. Next, we elucidated the principles governing FLS2-flg22 interactions and, thus, immunogenicity. We identified two distinct mutational tracks that rely on distinct mechanisms to avoid epitope detection by FLS2. One track drives a loss-of-agonist function by

reducing interaction with FLS2, while the second results in gain-of-function epitopes that act as FLS2 antagonists. Finally, a computational analysis of prevailing epitopes seen in the current bacterial sequence databases indicate that the changes resulting from these synthetic tracks exist in nature.

RESULTS

Deep mutational scanning of flg22 reveals the spectrum of amino acids required for motility and/or interaction with FLS2

To determine the extent to which the amino acid sequence of flg22 impacts the function of flagellin, we built a library of mutant bacterial strains expressing nearly all possible single missense mutations of the flg22 domain in *Pa* (*Pa flg22*). For this, we generated 412 *fliC* allelic clones by targeting all *Pa flg22* codons for replacement by codons that specify each of the other amino acids (Figure 1A). Next, we constructed a *Pa fliC* mutant (*Pa ΔfliC*) and transformed each individual clone of our mutant compendium into this nonmotile strain to test for motility rescue (Figures 1A, 1B, and S1A). To eliminate false negatives, we confirmed that the flagellin protein was expressed in all the transformants (Figure S1B). Only 18.7% of the strains displayed motility phenotypes indistinguishable from that of the wild-type *fliC* transformant (Figure S1C). While 45% of the transformants showed a markedly reduced motility, 34.8% remained nonmotile, similar to *Pa ΔfliC* (Figure S1C). Thus, the vast majority of the mutations in our deep mutational scan negatively impact motility in *Pa* (Figure 1C). In contrast, only a few mutations enhanced *Pa* motility (Figure 1D).

Based on the "address-message" concept (Meindl et al., 2000), supported and refined by the crystal structure of FLS2 in complex with Pa flg22 (Sun et al., 2013), the 22 amino acids of the epitope can be divided into two functional domains (Figure 1E). The "address" segment includes the seventeen N-terminal residues and interacts with FLS2. The last five C-terminal residues define a "message" segment that creates a docking site for the co-receptor BRI1-ASSOCIATED RECEPTOR KINASE 1 (BAK1) and thus is important for appropriate activation of immune responses (Belkhadir et al., 2014). We used flg22 sequence conservation and structure as well as the "address-message" concept to map the impact of each amino acid changes on motility (Figures 1E–1G). We found that mutations targeting the "message" portion of the epitope had little to no effect on motility (Figure 1G). Conversely, more than half of the residues in the "address" domain (10 out of 17; >58%) were highly intolerant to mutations and are thus critical for motility (Figure 1G). When superimposed on the flg22 domain of the flagellin atomic structure (Wang et al., 2017), we found that these residues distributed over two small clusters that contribute structurally to a helix-loop-helix transition (Figure 1F). Thus, alterations of these clusters are most likely constrained by the structural requirements necessary to build a functional flagellum. The amino acids of these clusters are well conserved in flg22 epitopes derived from naturally occurring strains of *Pseudomonads* (Figure 1E; Table S1; Data S1), and only 1.4% of the synthetic loss-of-function mutations identified here are found in wild Pseudomonas (Table S2; Data S1).
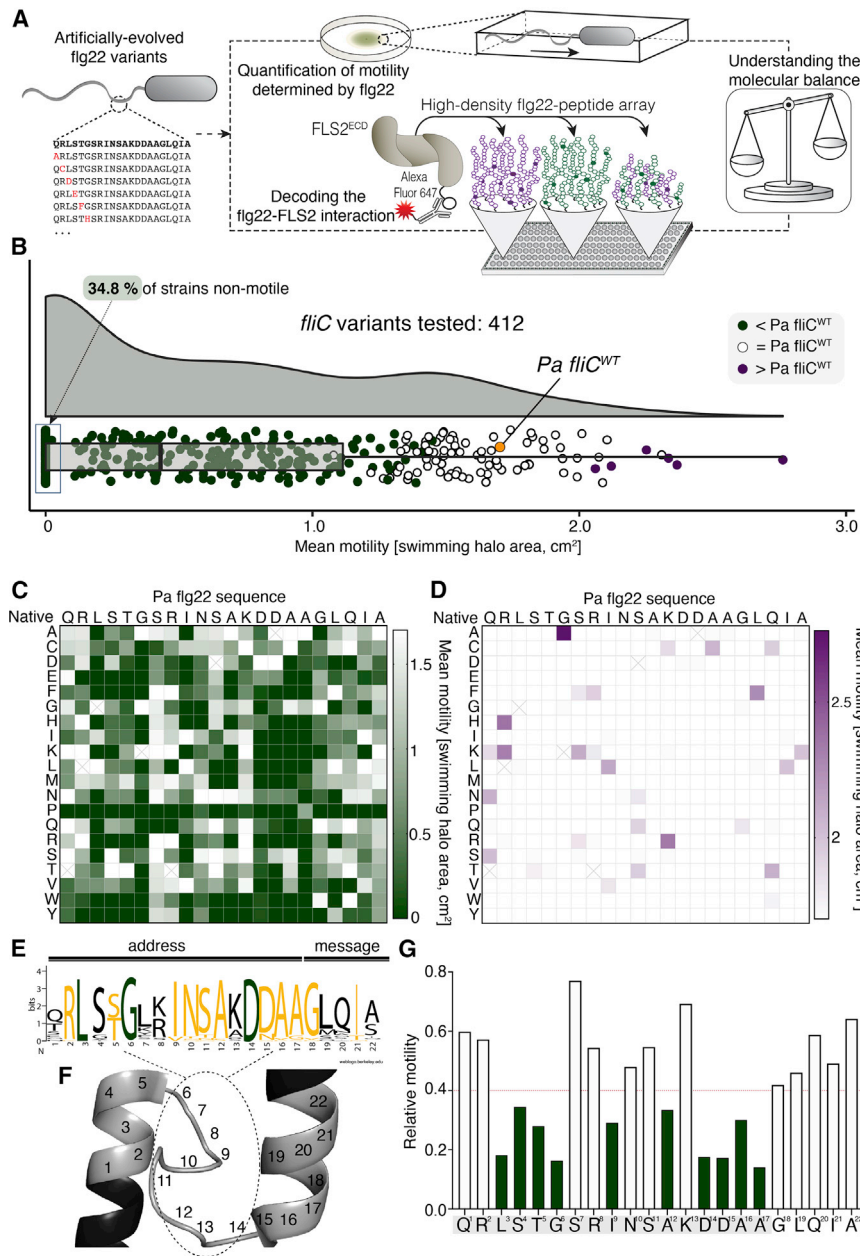
Figure 1. Deep mutational scans of flg22 underpin the spectrum of amino acids critical for bacterial motility

(A) Mutational scanning pipelines used in the study.

(B) Raincloud plot representing the density distribution of the mean swimming motility for Pa $\Delta fliC$ strains complemented with allelic variants of $fliC$. The box plot shows the median motility and the quantiles. Transformants with a significantly reduced or increased motility compared with wild type ($fliC^{WT}$, in orange) are indicated in green and purple, respectively (two-sided Mann-Whitney U test followed by a FDR correction; $p < 0.05$). Transformants with motilities comparable with $fliC^{WT}$ are indicated in white.

(C and D) Position-specific scoring matrix heatmaps representing the impact of amino acid substitutions on Pa motility. Reduced and increased motility is indicated in green (C) and purple (D) pixels, respectively. White pixels marked with a cross indicates amino acid substitutions that were not tested for motility.

(E) $Pseudomonads$ flg22 sequence logo. Invariant or highly conserved (with at most two substitutions) amino acids are highlighted in green and orange, respectively. The size of the letters indicates the conservation level of each amino acid in bits. The address/message segments and amino acids positions are indicated on top and bottom, respectively.

(F) Superimposition of flg22 (marked in gray) on flagellin structure (PDB ID: 5WK6). Amino acids numbers are indicated on the structure.

(G) Bar plots representing the relative motility (compared with wild type) resulting from all amino acid changes at each position. The red dotted line represents half of the maximum value for the least affected position S7. Positions with a relative motility below this line are marked in green.

Next, we predicted that FLS2 would focus on the conserved residues that are important for motility. To test this, we interrogated pairwise interactions between the extracellular domain of FLS2 (FLS2^{ECD}) and thousands of mutated flg22 peptides (Figure 1A). We used a high-density peptide array that comprised full substitution scans targeting both full-length Pa flg22 as well as epitope variants truncated at either or both of the N- and C-terminal moieties (Figures S2A–S2E). To test the full contribution of the "address/message" segments to the interaction with FLS2, we additionally deleted both extremities of Pa flg22 in a stepwise manner (Figures S2D and S2E). In total, we interrogated and assigned an interaction score to over 3,000 pairwise interactions between synthetic epitopes and FLS2^{ECD} (Figure S2A). Next, we focused on the peptides from the mutational scans of the full-

length epitope and used statistics relying on interquartile range (IQR) to assign their interaction scores to distinct categories (Figure 2A). Peptides with an interaction score below or above the IQR of the wild-type Pa flg22 controls were considered to have weaker or stronger interactions with FLS2^{ECD}, respectively (Figure 2A). All others were classified as having a similar interaction. Peptides with an interaction score 1.5 times above or below the Pa flg22 IQR were designated as significantly different (Figure 2A). Using these cutoffs, 23 peptide variants showed a significantly enhanced interaction with FLS2^{ECD}. Only flg22^{D14H} and flg22^{D14L} displayed a drastically reduced interaction (Figure 2A). Overall, 74.5% of the mutant peptide population retained interaction with FLS2^{ECD}. Thus, disrupting the stability of the flg22-FLS2 interaction by single amino acid replacement is difficult. We propose that, in Arabidopsis, the stability of this interaction counteracts bacterial attempts to evade immune detection through single amino acid substitutions.

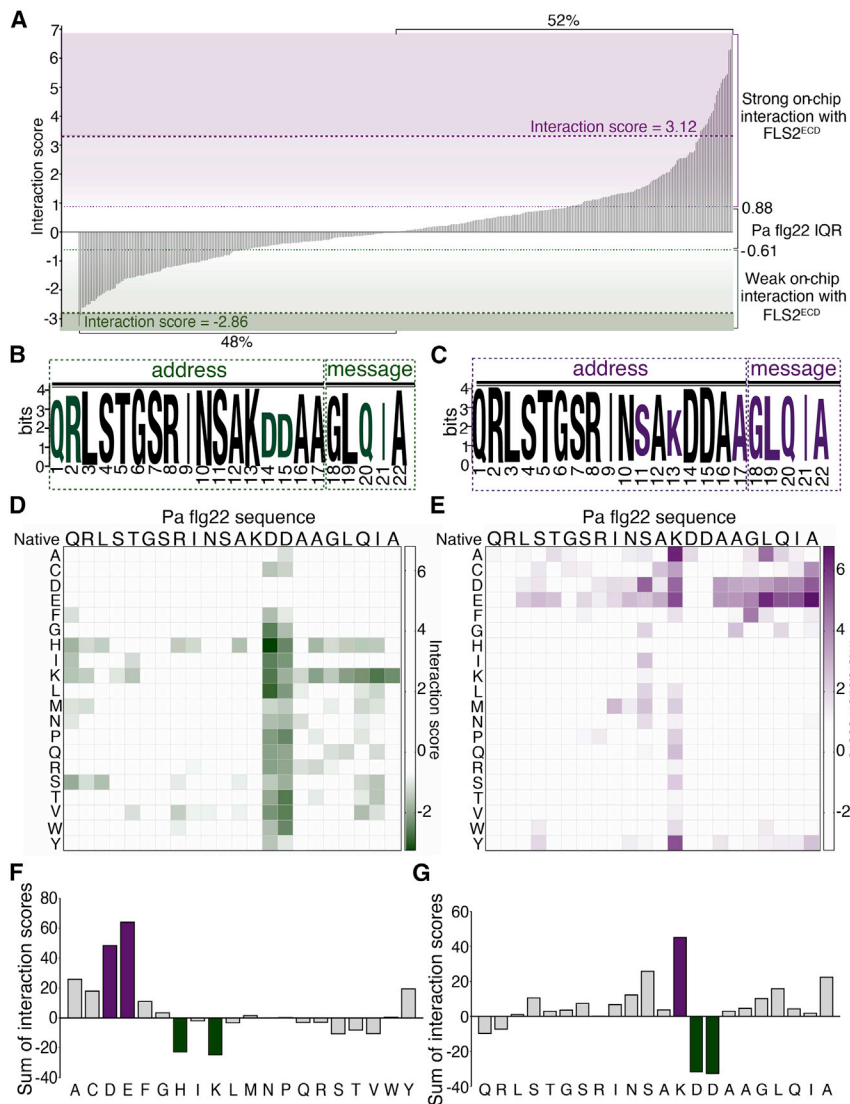We then leveraged our dataset and mapped the individual impact of all programed amino acid replacements on the flg2-

Figure 2. Deep mutational scans of flg22 determine the repertoire of amino acids controlling interaction with FLS2

(A) Distribution of interaction scores between FLS2[ECD] and flg22 peptides derived from the full-length mutational scans. flg22 peptides were classified as interacting with FLS2[ECD] more strongly (purple), similarly (white), or more weakly (green) based on analysis of the interquartile range (IQR). Peptides with an interaction score >3.12 or <−2.86 were designated as significantly different from all others.

(B and C) flg22 sequence logos mapping the FLS2 interaction scores. Amino acid mutations that reduce or enhance the strength of the flg22-FLS2[ECD] interaction are highlighted in green or purple, respectively. Small letters indicate a more reduced (B) or improved (C) interaction. The address/message segments and amino acids positions are indicated on top and bottom, respectively.

(D and E) Position-specific scoring matrix heatmaps representing the impact of each amino acid change on the flg22-FLS2[ECD] interaction. Mutations generating flg22 variants with FLS2 interaction scores below (D) or above (E) the IQR of the wild-type Pa flg22 are represented in green or purple pixels, respectively. White pixels indicate variants with an interaction score distributing within the Pa flg22 IQR.

(F) Bar plot representing the sum of interaction scores resulting from substitutions targeting all flg22 positions with the same amino acid.

(G) As in (F) but for all the substitutions at each amino acid position. For (F) and (G), substitutions that strongly reduce or enhance the interaction scores are marked in green or purple, respectively.

Antagonistic pleiotropy constrains the evolution of non-immunogenic flg22 variants

Next, we predicted that if selective forces acted antagonistically to fine-tune bacterial motility and/or interaction with FLS2, we should be able to detect their molecular footprints. To address this, we assigned, based on the interaction score of their respective epitopes, each individual bacterial mutant strain of our collection to one of the three interaction subgroups we previously defined (Figure 2A). We then analyzed the motility of each group and found that the density distribution between the interaction subgroups did not differ significantly (Figure 3A). Then, we compared the individual contribution of each residue to both motility and interaction with FLS2 (Figure S3A). We found that mutations of the invariant or highly conserved residues Leu[3], Gly[6], and Ala[16/17] retained near-wild-type levels of interaction with FLS2 while having drastic consequences on motility (Figure S3A). A second group of evolutionary conserved residues displayed no global adverse effects on either motility maintenance or FLS2 interaction (Figures 1C and S3A). Thus, evolutionary conservation is not the sole criteria used by FLS2 to detect this flagellin epitope in Arabidopsis.

FLS2[ECD] interaction (Figures 2B–2G). Mutations replacing any residue of the "message" segment with positively or negatively charged amino acids reduced or increased the flg22-FLS2[ECD] interaction, respectively (Figures 2B–2G). Similarly, exchanging Lys[13] for a negatively charged amino acid enhanced the interaction with FLS2[ECD] (Figures 2E and 2F). Thus, the local electrostatic charge of both the address and message segment of the epitope can either promote or disrupt the interaction with FLS2 (Figure 2G). Our analyses revealed that Asp[14] and Asp[15] (hereafter Asp[14/15]) are above all, independent of the peptide length, the most critical residues of the "address" segment for interaction with FLS2[ECD] (Figure S2F). Our findings are supported by structural and functional studies (Chinchilla et al., 2006; Sun et al., 2013). Despite the high conservation of other residues, the Arabidopsis FLS2 receptor focuses with extreme precision on the epitope's Asp[14/15] residues, likely because this doublet is important for structurally defining a boundary of the helix-loop-helix transition in the flg22 domain of flagellin (Figure 1F).
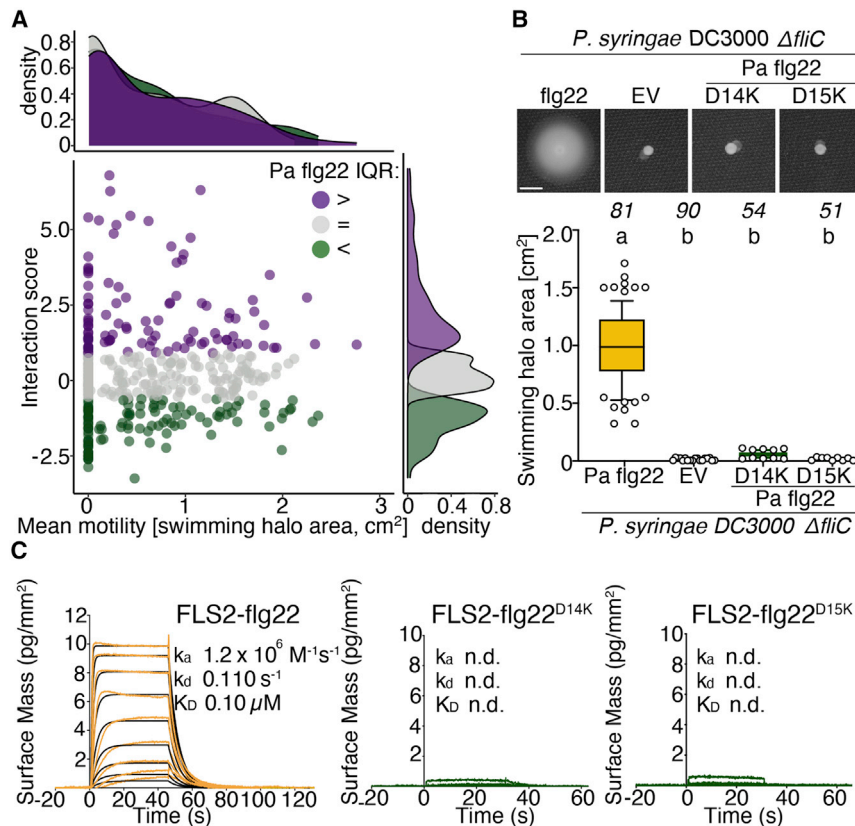
Figure 3. Antagonistic pleiotropy constrains the evolution of non-immunogenic flg22 epitopes

(A) Scatterplot representing the relationship between the overall motility of the *Pa* transformant compendium (x axis) and the flg22-FLS2 interaction scores (y axis). Each transformant was assigned to an interaction subgroup based on the Pa flg22 IQR and was color-coded accordingly. The margins indicate the density distributions color-coded by interaction subgroups. The density distributions of the subgroups are not statistically different (Kolmogorov-Smirnov test, KS > 0.6).

(B) Substitution of Asp[14/15] to a Lys disrupts the swimming motility of *Ps*. Top panel: pictures showing the motility phenotype of *Ps ΔfliC* strains complemented with an empty vector (EV) or with *fliC* variants coding either the flg22[D14K] or flg22[D15K] epitopes. Scale bar: 0.5 cm. Bottom panel: quantification of swimming motility for the indicated *Ps* strains. Genotypes with the same letter are indistinguishable at >95% confidence (one-way ANOVA followed by Tukey's HSD for all pairwise comparisons; p < 0.05). The number of biologically independent observations (n) is indicated on top of the graph.

(C) GCI-derived interaction kinetics of FLS2/flg22 interactions. Shown are sensorgrams with data in orange (Pa flg22) or green (flg22[D14K]/flg22[D15K]), with the respective fits overlaid in black. n.d. indicates not determined.

We found, however, that mutations of Asp[14/15] were able to disrupt both interaction with FLS2 and bacterial motility at a higher frequency than any other residue (Figures S3A–S3C). To confirm the broader implications of these results, we tested if mutations targeting Asp[14/15] would also disrupt the motility of the host-specific plant pathogen *Pseudomonas syringae* (*Ps*). We focused on flg22[D14K] and [D15K] because these substitutions clearly disrupted the interaction with FLS2[ECD]. First, we engineered the *Ps fliC* gene so that it encodes the Pa flg22 epitope and subsequently verified that the resulting gene complemented *Ps ΔfliC* motility (Figure S3D). We then used this engineered strain to independently introduce the missense mutations targeting the Asp[14/15] doublet. Motility assays on semisolid media, as well as live imaging in liquid conditions, demonstrated that neither of these two mutant strains moved (Figure 3B; Video S1). Next, we verified that these mutant epitopes no longer interacted with FLS2[ECD] in grating-coupled interferometry (GCI) assays (Hohmann et al., 2018) (Figure 3C). Thus, the adaptive fixation of the Asp[14/15] doublet for the maintenance of *Pseudomonads* motility is maladaptive in the presence of FLS2 and defines a typical signature of AP. We then reasoned that bacteria must have evolved ways to alleviate the antagonistic effects mediated by these two residues. Accordingly, a few strains in our synthetic collection had a set of overlapping mutations targeting Asp[14] or Asp[15] that allowed partial restoration of motility while still preventing maximal interaction with FLS2 (Figure S3C). Since these synthetic mutations can occur as natural variations of Asp[15] in pathogenic lineages of *Pseudomonas* that associate with

Arabidopsis in the wild (Tables S1 and S2; Data S1), we propose that carefully balanced trade-offs have occurred throughout evolution to maximize the escape from FLS2 detection while maintaining suboptimal flagellin function.

Functional uncoupling of FLS2 interaction from activation as a strategy to avoid immune responses

Next, we assessed the immunogenic functions of the mutant epitopes identified by our deep sequence/interaction mutational scans. For this, we selected, in addition to flg22[D14K] and [D15K], epitope derivatives that uniformly covered both ends of the FLS2 interaction score distribution (Figure S4A; Data S2 and S3). A total of 44 synthetic peptides, including ten of the variants that belonged to the group with a significantly enhanced interaction (SEI), were subsequently tested and systematically compared with the immunogenic responses of Pa flg22 in both wild type and *fls2* mutant plants (Figures 4A and S4B–S4F). All our assays also included the inactive Pa flg20 peptide as an additional negative control (Felix et al., 1999). We used flg22-induced reactive oxygen species (ROS) and seedling growth inhibition (SGI) assays to measure FLS2 activation and found that immune signaling was largely contingent on interaction with FLS2 (Figures 4A and S4B–S4F). Most of the variants with interactions comparable to Pa flg22 induced similar immune responses, although a few elicited slightly stronger or weaker responses. Only flg22[Q20C] had an interaction score that contrasted with its immunogenic activities and was therefore treated as an outlier (Figures S4G–S4K). We found that no epitopes from the
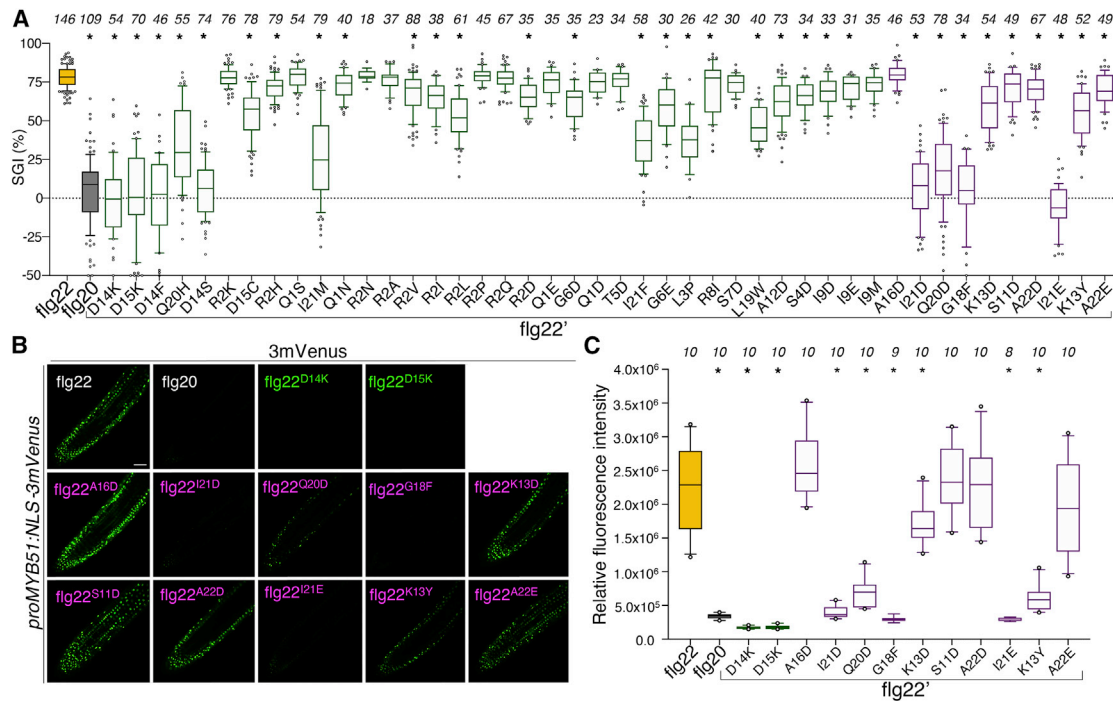
Figure 4. Uncoupling of FLS2 interaction from activation as a strategy to produce non-immunogenic flg22 epitopes

(A) flg22-induced seedling growth inhibition (SGI). Biologically independent observations (n) are indicated on top of the graph. The flg22 peptides tested are indicated at the bottom. The peptides are ordered from left to right by increasing interaction score with FLS2. Statistical significance was assessed using a linear mixed model (two-sided t-test followed by multiple testing correction using the Holm method; *p < 0.05).

(B) Root expression patterns of the defense marker gene *MYB51* in response to epitope treatments. Shown are images from single confocal sections. The epitopes are indicated on top of each panel. Scale bar shown for flg22 is 50 μm and applies to all pictures.

(C) Quantitative analysis of mVENUS signal intensities after treatment with the flg22 peptide derivatives indicated at the bottom. The number of biologically independent observations (n) is indicated on top of the graph. * indicates statistical significance (one-way ANOVA followed by a Dunnett's multiple comparison test; p < 0.05).

SEI group surpassed the responses induced by Pa flg22 (Figures 4A, S4C, S4D, and S4F). In fact, four of these variants displayed output responses that resembled that of flg20 (Figures 4A and S4B–S4F). Thus, we verified that these variants interacted with FLS2 using GCI (Figure S4L; Data S4).

To further confirm these results, we used live imaging of immune marker gene expression and monitored FLS2 responses in the epidermal cells of cotyledons and roots using two sets of fluorescent transcriptional reporter lines (Figures 4B, 4C, S4M, and S4N) (Wyrsch et al., 2015; Zhou et al., 2020). Consistent with our previous results, flg22D14K and D15K were not active in these assays (Figures 4B and 4C). flg22I21D, flg22Q20D, flg22I21E, and flg22G18F proved once more to be non-immunogenic in these assays, while all other SEI peptides displayed responses nearly equivalent to that of Pa flg22 in both cell types (Figures 4B, 4C, S4M and S4N). In contrast to flg22K13D, which induced a response in both root and cotyledons, flg22K13Y induced a response in cotyledon cells only (Figures S4M and S4N). Thus, FLS2 responses to polymorphic epitopes are cell type dependent in Arabidopsis. Collectively, our results show that interaction with, and activation of, FLS2 can be uncoupled. These findings are consistent with the uncoupling of FLS2 responses mediated by natural polymorphisms in commensal flg22 epitopes (Colaianni et al., 2021). We propose that this functional un-

coupling could be leveraged by microbes to circumvent the pressure of AP on the Asp14/15 residues.

Tunability of antagonistic pleiotropy in the message segment of flg22 licenses the evolution of non-immunogenic epitopes

Next, we assessed whether the mutations defined in the group of non-immunogenic SEI peptides (hereafter niSEI) affected the motility of either Pa or Ps using the same strategy as described above. We found that strains encoding FliC variants with either the flg22I21D or flg22G18F epitopes restored motility of Pa ΔfliC to half of the levels of the unmutated FliC, while strains carrying flg22Q20D and flg22I21E failed to do so (Figures 5A and S5A). In contrast, these gene variants acted in opposite ways in the rescue of Ps ΔfliC (Figures 5B and S5B; Video S1); strains encoding FliC variants carrying the flg22Q20D and flg22I21E epitope were able to move as well as strains carrying Pa flg22. Notably, all immunogenic variants from the SEI subgroup rescued the motility to at least half of the levels of the wild-type control (Figures S5C and S5D). As a co-receptor, BAK1 recognizes the Gly18 and Leu19 residues of the FLS2-bound flg22 (Sun et al., 2013). Since these residues are in the vicinity of Gln20 and Ile21, we investigated how the perception of all the SEI variants impact FLS2-BAK1 interaction *in vitro* (Smakowska-Luzan et al.,
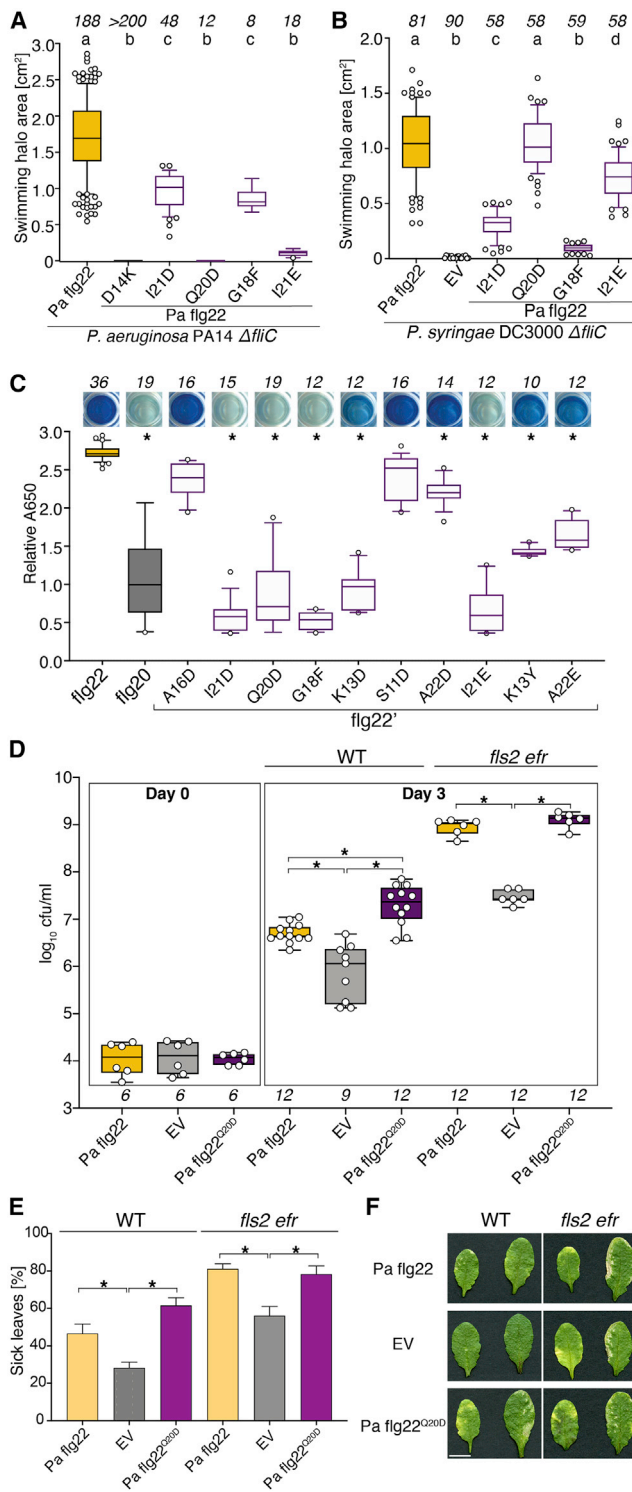
Figure 5. The tunability of antagonistic pleiotropy in the message segment of flg22 impacts the FLS2-BAK1 interaction and provides host colonization advantages

(A and B) Quantification of swimming motility for *Pa* (A) and *Ps* (B) *Δ fliC* strains transformed either with an EV or with *fliC* variants coding Pa flg22, or the niSEI flg22 variants. Genotypes with the same letter are indistinguishable at >95% confidence (one-way ANOVA followed by Tukey's HSD for all pairwise comparisons; $p < 0.05$).

2018). We found that all the niSEI peptides failed to trigger maximum heterocomplex formation, while the SEI peptides did not (Figure 5C). Thus, specific amino acid substitutions at position 18, 20, or 21 resolve AP by modulating the FLS2-BAK1 interaction. Notably, the change at position 20 offered a full bypass of AP in *Ps* (Figure 5B). Accordingly, *Ps* strains encoding a FliC variant carrying the flg22^{Q20D} epitope were able to colonize Arabidopsis significantly better than strains carrying Pa flg22 and inflicted more disease symptoms (Figures 5D–5F). Since the changes at position 18, 20, or 21 did not affect the motility of *Pa* and *Ps* equally, we propose that the tunability of AP is dependent on the bacterial species considered.

Synthetic evidence for receptor antagonism as a strategy to dampen immune responses

Next, we obtained *in vitro* binding kinetics using GCI and determined that all the niSEI peptides induced unstable FLS2-BAK1 complexes (Figures 6A and S6A; Data S4). We confirmed these results *in vivo* by using co-immunoprecipitation assays (Figure 6B). The FLS2/BAK1 interaction leads to the phosphorylation of the cytoplasmic kinase BOTRYTIS-INDUCED KINASE 1 (BIK1) for downstream signaling (Kadota et al., 2014; Lu et al., 2010; Wang et al., 2018). None of the niSEI peptides induced BIK1 phosphorylation (Figure S6B). Surprisingly, flg22^{A22E} triggered BIK1 phosphorylation without inducing FLS2-BAK1 interaction *in vivo* (Figures 6B and S6B). Thus, discrete polymorphic changes in flg22 can uncouple the responses of FLS2 in Arabidopsis. We propose that this uncoupling involves a regulatory mechanism that is yet to be identified. Consistent with this hypothesis, a subset of commensal flg22 epitopes disconnect the signaling outputs of FLS2 (Colaianni et al., 2021).

Next, we tested if the niSEI peptides could negate Pa flg22-induced activation of the immune marker gene *Cytochrome P450 71A12* (*CYP71A12*) (Millet et al., 2010). Using a transcriptional reporter system, we determined that, except for flg22^{G18F}, all the niSEI peptides antagonized the induction of *CYP71A12* by Pa flg22 (Figure S6C). In contrast, epitopes that interacted less with FLS2, were not able to block the induction of *CYP71A12* by Pa flg22 (Figure S6C). We then tested if flg22^{Q20D} and flg22^{I21D} antagonized the formation of the FLS2-BAK1

(C) FLS2-BAK1 heterocomplex formation measured *in vitro* using an enzyme-linked immunosorbent assay. Represented is the relative absorbance (A650 nm) over 2 h. Representative pictures of wells are shown on top. For (A–C) the number of biologically independent observations (n) is indicated on top of each graph.

(D) Growth of *Ps ΔfliC* strains transformed either with an EV or with *fliC* variants coding Pa flg22, or flg22^{Q20D} on the plant genotypes indicated on top. The number of bacteria per area of leaf (cfu/mL) is plotted on a $\log_{10}$ scale for day 0 and day 3. Dots represent individual observations from two independent experiments. n = numbers of samples is shown at the bottom (8 leaf disks from 4 plants/sample).

(E) Quantification of leaf disease symptoms using the bacterial strains and plant genotypes described above. For (C–E) * indicates statistical significance (one-way ANOVA followed by a Dunnett's (C) or Sidak (D and E) multiple comparison test; $p < 0.05$).

(F) Representative pictures of leaves taken 5 days after inoculation with the bacterial strains described above. Plant genotypes indicated on top. Scale bar: 1 cm.
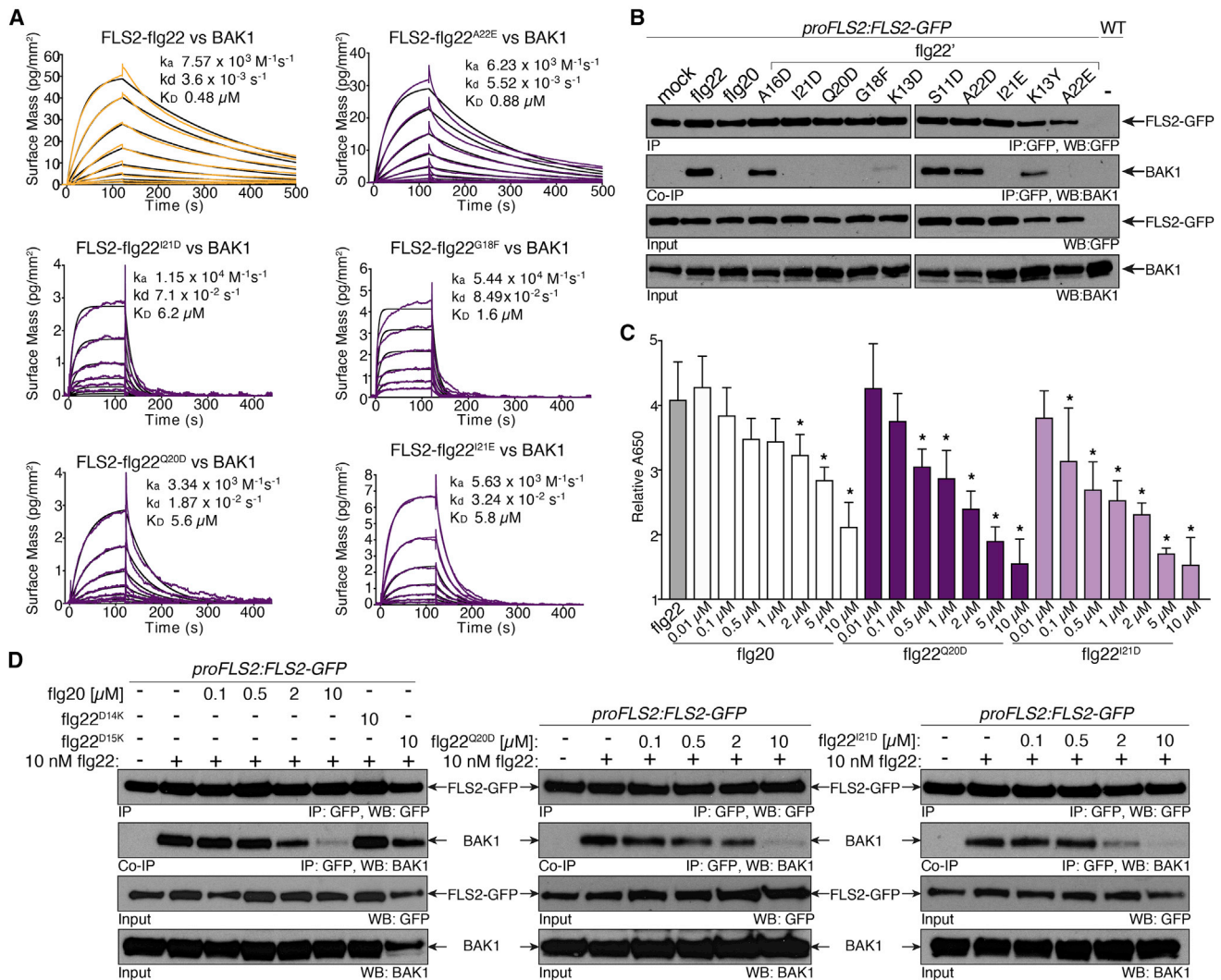
Figure 6. Competitive antagonism of receptor complex formation as a path to dampen immunity

(A) GCI-derived binding kinetics for the flg22-bound FLS2 and BAK1. Shown are sensorgrams with data in orange and purple with the respective fits overlaid in black. The association (k_a) and dissociation (k_d) rate constants and the dissociation constant K_D are shown in the charts.

(B) Western blot analyses of FLS2-BAK1 co-immunoprecipitations (coIP/IP) in Arabidopsis transgenic seedlings (*proFLS2:FLS2-GFP*) either left untreated or treated for 10 min with different flg22 peptides.

(C) FLS2-BAK1 heterocomplex formation measured *in vitro* using an enzyme-linked immunosorbent assay. Represented is the relative absorbance (abs 650 nm) over 2 h obtained in the presence of Pa flg22 (10 nM) alone or at increasing concentrations of flg20, flg22^{Q20D}, or flg22^{I21D}. * indicates statistical significance (one-way ANOVA followed by a Dunnett's multiple comparison test; $p < 0.05$).

(D) Western blot analyses of FLS2-BAK1 co-immunoprecipitations (Co-IP/IP) in Arabidopsis transgenic seedlings (*proFLS2:FLS2-GFP*) either left untreated, treated with Pa flg22 peptide (10 nM) alone, or co-treated with different flg22 peptides at the concentrations indicated on top. The identity of the flg22 peptides is indicated on the left. This experiment was repeated two times with similar results.

heterocomplex induced by Pa flg22 *in vitro* (Figure 6C). We determined that both peptides readily inhibited this interaction at concentrations fifty times higher than Pa flg22. In contrast, Pa flg20 required a 200-fold molar excess, to achieve the same level of antagonism. Finally, we demonstrated that flg22^{Q20D} and flg22^{I21D}, but not flg22^{D14K} or flg22^{D15K}, antagonized the flg22-induced FLS2-BAK1 interaction *in vivo* (Figure 6D). Thus, we synthetically evolved antagonistic flg22 epitopes that inhibit the activation of downstream FLS2 responses with no apparent effect on motility.

Acquisition of antagonist peptide function as a natural strategy to poison FLS2 function

In the next step, we looked for the occurrence of the substitutions identified by our synthetic approaches in natural lineages of *Pseudomonas*. We found that Asp^{15}, but not Asp^{14}, occurred as Gly (flg22^{D15G}) or Asn (flg22^{D15N}) in *Pseudomonas fluorescens* and *Ps* pathovars that associate with plants (Winsor et al., 2016). Since both mutations reduced the motility of *Pa* (Figure S3C), we hypothesized that variations of the Asp^{15} residue would perhaps be accompanied by concomitant changes that compensate the

presumed motility defect. To test this, we used mutual information theory (MIT) to analyze the co-occurrence of polymorphisms in FliC protein sequences extracted from the general Pseudomonas Genome Database (Figure 7A; Table S3) (Gouveia-Oliveira and Pedersen, 2007; Winsor et al., 2016). We found that co-variation between positions 15 and both 17 and 18 in the flg22 segment distributed in the top 0.5% of MIT scores (Figure 7A). We retrieved two representative epitopes with these co-variations and focused on them for experimental validation. These epitopes had additional polymorphisms in the "address" and "message" segments and were named flg22^{GDG} (Gly^{15}/Asp^{18}/Gly^{20}) and flg22^{NSS} (Asn^{15}/Ser^{17}/Ser^{22}). Then, we set out to understand the functional impact of this polymorphism on immunogenicity (Figure 7B). As controls, we generated chimeric peptides (flg22^{chGDG} and flg22^{chNSS}) in which the message segments were fused to the address of Pa flg22 and subsequently tested their ability to induce ROS bursts and FLS2-BAK1 interaction in vitro (Figures 7B and S7A). While flg22^{NSS} and flg22^{chNSS} induced normal FLS2/BAK1 interactions and wild-type ROS bursts, flg22^{GDG} and flg22^{chGDG} were unable to do so (Figures 7B and S7A). The results obtained for flg22^{NSS}/flg22^{chNSS} imply that co-variation between positions 15 and 17 is perhaps not sufficient to avoid the induction of FLS2 responses in Arabidopsis.

To understand why flg22^{chGDG} is non-immunogenic, we synthesized Pa flg22 peptides in which the substitutions were introduced separately (flg22^{D15G}, flg22^{G18D} and flg22^{Q20G}) or in pairwise combinations (flg22$^{D15G/G18D}$, flg22$^{D15G/Q20G}$, and flg22$^{G18D/Q20G}$) and tested ROS responses (Figure 7C). The ROS bursts mediated by flg22^{D15G} were indistinguishable from that of Pa flg22. These results are supported by the slight reduction in FLS2 interaction observed on our peptide array for this variant (Figure 2D). Remarkably, flg22^{G18D} and flg22^{Q20G} induced lower ROS burst responses than Pa flg22, and these responses were further decreased when the mutations occurred together (flg22$^{G18D/Q20G}$) or jointly with flg22^{D15G} (Figure 7C). Thus, we propose that positive epistatic interactions between these residues occur to greatly reduce epitope immunogenicity. Next, we reasoned that the introduction of a negative charge at position 18 should rescue the slight reduction in FLS2 interaction for flg22^{D15G}. Second, we expected that the introduction of this negative charge together with the change at position 20 would result in a molecular phenocopy of the niSEI epitopes flg22^{G18F} and flg22^{Q20D} (Figures 5C, 6C, and 6D), thereby allowing flg22^{GDG} to antagonize the Pa-flg22-induced FLS2-BAK1 interaction. As expected, flg22^{GDG} and its corresponding chimera failed to trigger FLS2-BAK1 heterocomplex formation, and antagonized the activities of Pa flg22, both in vitro and in vivo (Figures 7D, 7E, S7A, and S7B). We propose that positive epistasis not only channels the positive pressure acting to mediate evasion from FLS2 detection in Arabidopsis but also dampens plant immune system function by poisoning the activity of FLS2-BAK1 heterocomplexes with antagonist epitopes.

To establish the effects of positive epistasis on flagellin function, we assessed the impact of the flg22^{GDG} polymorphism on the motility of Pa and Ps either individually or collectively (Figures 7F, S7C, and S7D). While FliC variants with flg22^{GDG} epitopes failed to rescue either Pa and Ps ΔfliC, the chimera restored 12.5 % of motility of Ps but not in Pa (Figures 7F and S7D). These results reinforce the notion that the tunability of motility is spe-

cies dependent (Figures 5A and 5B). When introduced separately, each of the mutations restored 18.5% of the motility of Pa ΔfliC (Figure S7C). Thus, the residues 15, 18, and 20 can interact negatively to control Pa motility. Control complementation assays performed with flg22^{NSS} derivatives yielded nearly similar results (Figures 7F and S7D) and further indicated that Pseudomonas motility is very sensitive to residue co-variations in flg22. The natural polymorphism at position 20 (flg22^{Q20G}), as for the niSEI peptide flg22^{Q20D} (Figure 5B), offered the most balanced resolution of AP (Figures 7C and S7B). Altogether, our results indicate that positive epistatic interactions mediating evasion from immune system detection lead to negative effects on flagellin function. We propose that flg22^{GDG}-like polymorphisms could eventually persist on Arabidopsis because the benefits of reducing immune system detection via antagonist activity outweighs the negative effects on motility function.

In support of this, we found that the flg22^{GDG} allele occurred in the genomes of Pseudomonas operational taxonomic units (Ps OTUs) that stably associate with Arabidopsis in the wild (>1,500 genomes; Karasov et al., 2018). Because the flg22^{GDG} allele occurs at a very low frequency in these genomes (<0.1%; Table S4; Data S1), we propose that this allele is nonadaptive for Arabidopsis colonization. In contrast, we found that >85% of these genomes encoded two distinct flg22 epitopes reminiscent of the antagonist niSEI peptides, with changes present at position 20 and 21 (Table S4). In addition to these substitutions, a bit less than half of the OTUs genomes analyzed with the MIT algorithm showed co-variation between position 15 and 18 in flg22 (Figures S7E and S7F; Table S5). Thus, we used co-variation as a criterion to classify these peptides; the flg22 peptide with co-variation between Asn^{15} and Val^{18} accompanied by substitutions at positions 20 and 21, was named Var I (flg22$^{V.I}$) (Figure S7E); the other peptide with only substitutions at positions 20 and 21 was named Var II (flg22$^{V.II}$) (Figure S7E). In ROS burst assays both epitopes proved non-immunogenic (Figure S7G). This is consistent with previous results showing that Var I do not induce SGI (Vetter et al., 2016). Importantly, the change into Asn^{15} in the context of the Pa flg22 sequence did not affect ROS bursts responses (Figure S7G). Thus, substitutions at position 15 do not necessarily impact FLS2 responses. Rather, we propose that the loss of immunogenic function in Var II is mediated by the changes at position 20 and 21. Based on the data obtained for the niSEI and flg22^{GDG} epitopes, we hypothesized that Var I and Var II would both act as FLS2 antagonists. Expectedly, Var I and Var II reduced Pa-flg22-induced FLS2-BAK1 interaction in vivo, albeit with different strengths (Figure S7H). When compared with Var II, Var I more strongly inhibited Pa-flg22-induced FLS2-BAK1 complex formation (Figure S7H). Our results are supported by the antagonistic effects of Var I and Var II on Pa flg22 induction of CYP71A12 (Colaianni et al., 2021). We propose that the co-variation between positions 15 and 18 in Var I interacts positively with the changes at positions 20 and 21 to increase antagonist function. Because single substitutions to Asn^{15} or to Val^{18} in Pa flg22 reduce the motility of Pa by approximately 70% (Figure S7I), it is likely that the polymorphism of Var I and Var II leads to reduction in motility. Alternatively, this motility reduction is either minimally adaptive and/or compensated by co-evolving sites outside the epitope segment (Figure S7F). We hypothesize that the reduction of
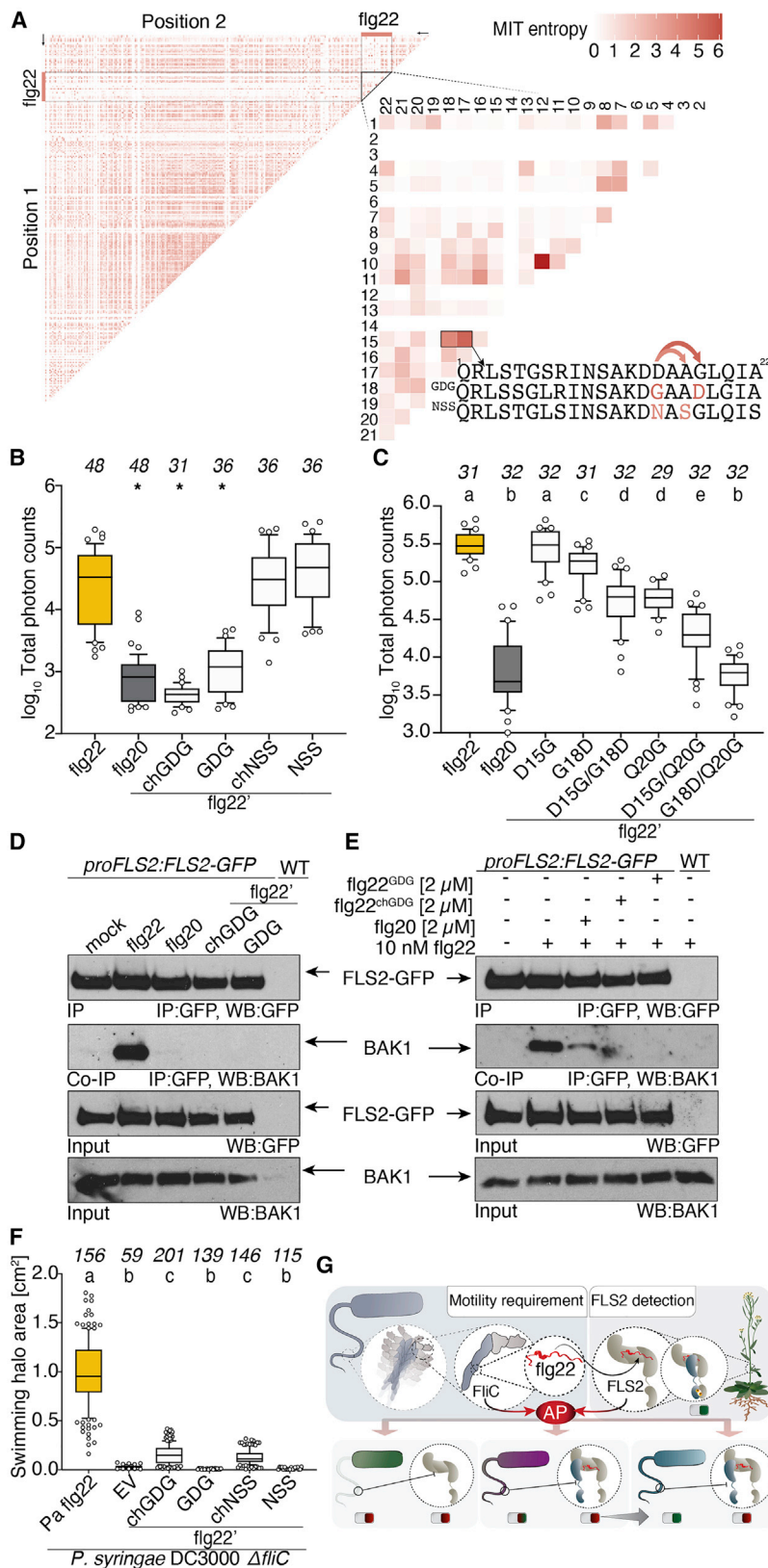
Figure 7. Natural occurrence of antagonist epitope function in *Pseudomonads*

(A) Mutual information theory (MIT) heatmap of FliC protein sequences from the Pseudomonas Genome Database. The flg22 segment is magnified on the right. The color scalebar on top shows the MIT entropy score values between positions. The arrows on the flg22 sequence at the bottom indicate that Asp[15] co-varies with Ala[17] (flg22[NSS]) or Gly[18] (flg22[GDG]).

(B and C) flg22-induced oxidative bursts represented as total photon counts over 40 min. Pa flg22, flg22[GDG], flg22[NSS], and the respective chimeras flg22[chGDG]/flg22[chNSS] (B) along with peptides that recapitulate different combinations of single and pairwise polymorphism in flg22[chGDG] variant (C) were used at a concentration of 100 nM. For (B) * indicates statistical significance (one-way ANOVA followed by a Dunnett's multiple comparison test; p < 0.05).

(D) Western blot analyses of FLS2–BAK1 coIP/IP in Arabidopsis transgenic seedlings (*proFLS2:FLS2-GFP*) either untreated (mock) or treated for 10 min with the flg22 peptides indicated on top.

(E) Same as (D) except that the seedlings were treated with 10-nM Pa flg22 alone or co-treated with 10-nM Pa flg22 and 2 μM of flg22[GDG]/flg22[chGDG].

(F) Quantification of swimming motility of *P. syringae ΔfliC* strains transformed either with an EV or with *fliC* variants coding either Pa flg22, flg22[GDG], flg22[NSS] or the respective chimeras flg22[chGDG] /flg22[chNSS].

(C and F) Peptides and genotypes with the same letter are indistinguishable at >95% confidence (one-way ANOVA followed by Tukey's HSD for all pairwise comparisons; p < 0.05). The number of biologically independent observations (n) is indicated on top of each graph.

(G) Model depicting the role of AP on the functionality of FliC. AP maintains allelic diversity in flg22 by balancing the negative pressure to maintain FliC function against the positive pressure to evade FLS2 detection. Resolution of AP leads to (1) epitopes with reduced agonist function and dramatic reduction in motility (green bacteria) or to (2) epitopes with antagonist function and moderate reduction of motility (purple bacteria). Natural resolution of AP occurs through similar mechanisms (blue bacteria).

FLS2 function via antagonist activity has taken priority over the maintenance of motility in the *Ps* OTUs, thereby contributing to the dominance of this lineage on Arabidopsis.

Next, we sought for genomic evidence supporting that the design of epitopes with FLS2-BAK1 antagonist activities could provide widespread advantages for Arabidopsis colonization. For this, we analyzed the polymorphism of *FLS2* and *BAK1* in genomes of >1,000 natural Arabidopsis accessions (Alonso-Blanco et al., 2016). Our analysis revealed that >100 non-synonymous changes can occur in FLS2^{ECD} (Table S6). Of these, 41 substitutions involved amino acids located in leucine-rich repeats (LRRs) that contribute directly to interaction with flg22 (LRR2-16) (Sun et al., 2013). Arabidopsis possibly uses this variation to refine FLS2 selectivity for distinct types of epitopes. Consistent with this, FLS2 exhibit distinct epitope selectivity in land plants (Fürst et al., 2020; Robatzek et al., 2007; Takai et al., 2008; Trdá et al., 2014; Wei et al., 2020). In contrast to FLS2^{ECD}, polymorphism in BAK1^{ECD} is nearly non-existent, and only one non-synonymous change occurs in the extracellular juxtamembrane domain (Table S6). BAK1 physically interacts with over 30 receptor kinases to regulate other immune and developmental pathways (Boutrot and Zipfel, 2017; Hohmann et al., 2017; Smakowska-Luzan et al., 2018). Since single amino acid changes in the BAK1^{ECD} can disrupt the functioning of important signaling pathways (Jaillais et al., 2011), we attribute the lack of polymorphism to this "hub" function. Based on this, we posit that dominant isolates from the *Ps* OTUs have evolved to make FLS2 polymorphism irrelevant by exploiting the constrained "hub" function of BAK1 in Arabidopsis. This is consistent with our demonstration that >85% of these Arabidopsis isolates encode epitopes that antagonize the activities of Pa flg22 on the FLS2-BAK1 heterocomplex. The acquisition of flg22 epitopes with antagonist function is not limited to *Pseudomonads* but can also occurs in alpha- and betaproteobacteria that are found in the Arabidopsis microbiomes (Colaianni et al., 2021).

DISCUSSION

Evolutionary mechanisms that help explain how natural bacterial communities maintain core microbial functions while circumventing immunity are scarce (Teixeira et al., 2019), mainly because direct molecular evidences are challenging to obtain experimentally. Here, we demonstrate that AP refines the relationship between an epitope and an immune sensor and, in turn, show that trade-offs between bacterial motility and host recognition have been molecularly balanced throughout evolution.

The motility function encoded in flg22 is selectively monitored by FLS2

Our results indicate that >300 single alterations of flg22 have a drastic impact on *Pa* motility. Collectively, our data demonstrate that flg22 has, to a greater extent than anticipated, a coding function that massively impinges on *Pseudomonads* motility whereby amino acid changes targeting less-conserved residues also caused drastic motility defects. Conversely, mutations of some invariant amino acids had no obvious effects on motility. Thus, the evolutionary fixation of residues in the epitope is unlikely to be driven by selective mechanisms aimed only at maintaining bacterial motility. Our systematic analysis of flg22-FLS2

interactions allowed us to determine that in Arabidopsis, FLS2 did not evolve to monitor all the epitope positions that are necessary for motility. We propose that natural Arabidopsis accessions have evolved this capacity in their flagellin sensor to fine-tune and prioritize their defense responses against different bacteria. Consistent with this, natural flg22 epitopes induce diverse immune responses (Colaianni et al., 2021).

FLS2 resiliently interact with mutated flagellin epitopes

The directed evolution of >1,000 epitopes has produced insights that expand our understanding of the FLS2/flg22 interaction in important ways. Although our data are mostly aligned with the crystallographic data (Sun et al., 2013), we have found that, except for mutations targeting the Asp$^{14/15}$ doublet, Gln^{20} and Ile^{21}, all other mutations targeting residues with side chains that physically interact with FLS2^{ECD} in the crystal structure had no major impact on the interaction. Most notably, this robust interaction is only modulated by the introduction of residues with opposed electrostatic charges in the C-terminal moiety of the epitope. Remarkably, these electrostatic effects were magnified on 15-mer derivatives of the epitope that are universally recognized as immunogenic by FLS2 orthologs in flowering plants (Bauer et al., 2001; Felix et al., 1999; Robatzek et al., 2007). Overall, we propose that in Arabidopsis the robust interactions of FLS2 with mutated flagellin epitopes establishes AP and contributes to the maintenance of flagellin epitope variation in bacterial populations (Colaianni et al., 2021).

Antagonistic pleiotropy reduces the potential adaptive value of FliC

An obvious regulatory solution to the problem of AP would be to simply eliminate *fliC*. However, the genetic elimination of *fliC* in various plant-associated bacteria significantly reduces their virulence (Cesbron et al., 2006; Chesnokova et al., 1997). Bacteria employ other mechanisms to provide resolution of AP. One tactic deployed by several *Pseudomonads* involves degradation of excess flagellin monomers by secretion of proteases in the extracellular space (Bardoel et al., 2011; Pel et al., 2014). Another tactic relies on flagellin glycosylation (Taguchi et al., 2010). In some plant-specific bacteria, the addition of unique glycan structures prevents the appropriate release of epitopes, thereby leading to non-immunogenic flagellins (Buscaill et al., 2019). The most direct resolution of AP could be provided by the positive selection pressure driving discrete levels of polymorphism in the flg22 sequence (Felix et al., 1999; McCann et al., 2012; Mott et al., 2016; Sun et al., 2006). Yet, only a few pathogenic species seem to utilize this strategy because reductions in motility are suboptimal for host adaptation. In comparison, a relatively high level of polymorphism is maintained in commensal communities (Colaianni et al., 2021). This may indicate that these communities are less dependent on flagella-mediated motility and/or maintain multiple *fliC* copies in their genomes to resolve AP (Colaianni et al., 2021). Alternatively, immune suppression strategies such as these mediated by the type III secretion system and its effector proteins could be used to alleviate pressure on *fliC* or on any other MAMP-coding gene. In this strategy, however, resolution of AP would only be transferred to other processes since bacterial effectors are also robustly detected by plants Nod-like receptors (Laflamme et al., 2020).

Mutational scenarios for the acquisition of antagonist epitopes in *Pseudomonads*

We have identified mutational tracks in a flagellin epitope that drive plant immune system evasion and poisoning by antagonist production (Figure 7G). We found signatures of these tracks to be layered atop each other in naturally occurring bacteria that associate with Arabidopsis in the wild. Although we cannot precisely determine how these mutational signatures emerged, we propose that they were acquired through continuous series of mutagenic events. First, we envision that natural selection directed evasion from immune system detection and, as a consequence, stalled evolution by establishing AP. A second series of selection events only parsimoniously resolved AP but led to epitopes that reduce immune detection via antagonistic function. This newly acquired function persisted because it provides greater benefits for bacterial colonization than a mere restoration of motility (Figure 7G). Among others, a likely scenario could have included some of the following events: (1) natural selection has favored specific substitutions at position 15 in a background of mutations targeting other residues in the message segment (e.g., position 20), hence, resulting in bacteria retaining adaptive levels of motility while carrying epitopes with suboptimal reductions in immunogenicity, (2) the strong negative selection on BAK1 in Arabidopsis channeled frequent parallel co-variation between positions 15 and 18, and beneficial epistatic interactions between these residues and the residue at position 20 allowed a full reduction in epitope immunogenicity, (3) together these substitutions are also beneficial because they generate weak receptor antagonists and as such prevent an over titration of BAK1 function on other MAMP responses, hence, allowing harmonious microbiome assembly by avoiding "over-colonization" of the host by other competing species (Lee and Belkhadir, 2020; Smakowska et al., 2016), and (4) despite drastic effects on motility, this combination of substitutions was positively selected to allow bacteria carrying such epitopes to persist on Arabidopsis. Since the polymorphism at position 20 can offer a balanced resolution of AP in *Ps*, substitutions that occurred first at position 20 (or in other key residues of the "message" segment) and were followed by co-variations at positions 15 and 18 are also conceivable. In support of this second scenario, position 20 is the most polymorphic in flg22 epitopes encoded by *Ps* OTUs strains.

All in all, we provide a rationale to better understand the molecular evolution of other MAMP-receptor pairs in plants but also in lower and higher metazoans. For instance, our study could be used as a template to dissect how bacterial protein synthesis mediated by the elongation factor Tu (EF-Tu) has evolved in the face of recognition by the Brassicaceae-specific EF-Tu receptors (EFR) (Boutrot and Zipfel, 2017). Understanding how sequence variation in EF-Tu epitopes has been influenced by AP to avoid immune detection, while maximizing ribosome function during the elongation phase of translation would be of great interest. As a whole, the concept explored here has the potential to reframe our evolutionary understanding of non-self perception.

STAR★METHODS

Detailed methods are provided in the online version of this paper and include the following:

AUTHOR CONTRIBUTIONS

Project administration, Y.B.; conceptualization, K.P., N.G., C.D.J., J.L.D., and Y.B.; investigation, K.P., N.R.C., H.S.L., U.H., N.E., A.T., Z.B., D.L., and E.S.; supervision, K.P., C.D.J., J.L.D., M.H., U.B., N.G., C.B., and Y.B.; methodology, K.P., U.H., M.H., E.S., N.R.C., C.D.J., and Y.B; resources, M.M., A.M., Z.M.P., U.B., N.S., C.B., A.K., N.G., C.D.J., J.L.D., and Y.B.; software, N.R.C., C.D.J., and A.K.; formal analysis, N.R.C., K.P., I.R.A., and A.K.; validation, K.P., N.R.C., C.D.J., J.L.D., and Y.B.; writing—original draft, K.P. and Y.B.; writing—review and editing, N.R.C., C.D.J., J.L.D., U.H., M.H., and N.G., all other authors commented and agreed on the manuscript; visualization, K.P. and Y.B.

DECLARATION OF INTERESTS

J.L.D. is a co-founder of, and shareholder in, AgBiome LLC, a corporation whose goal is to use plant-associated microbes to improve plant productivity.

INCLUSION AND DIVERSITY

One or more of the authors of this paper self-identifies as an underrepresented ethnic minority in science. One or more of the authors of this paper self-identifies as living with a disability.

REFERENCES

1001 Genomes Consortium. (2016b). 1,135 Genomes reveal the global pattern of polymorphism in Arabidopsis thaliana. Cell *166*, 481–491.

Allen, M., Poggiali, D., Whitaker, K., Marshall, T.R., and Kievit, R.A. (2019). Raincloud plots: a multi-platform tool for robust data visualization. Wellcome Open Res. *4*, 63, https://doi.org/10.12688/wellcomeopenres.15191.1.

Alonso-Blanco, C., Andrade, J., Becker, C., Bemm, F., Bergelson, J., Borgwardt, K.M., Cao, J., Chae, E., Dezwaan, T.M., Ding, W., et al. (2016). 1,135 Genomes Reveal the Global Pattern of Polymorphism in Arabidopsis thaliana. Cell *166*, 481–491.

Barbier, M., and Damron, F.H. (2016). Rainbow vectors for broad-range bacterial fluorescence labeling. PLoS One *11*, e0146827.

Bardoel, B.W., van der Ent, S., Pel, M.J.C., Tommassen, J., Pieterse, C.M.J., van Kessel, K.P.M., and van Strijp, J.A.G. (2011). Pseudomonas evades immune recognition of flagellin in both mammals and plants. PLoS Pathog. *7*, e1002206.

Bauer, Z., Gómez-Gómez, L., Boller, T., and Felix, G. (2001). Sensitivity of different ecotypes and mutants of Arabidopsis thaliana toward the bacterial elicitor flagellin correlates with the presence of receptor-binding sites. J. Biol. Chem. *276*, 45669–45676.

Belkhadir, Y., Yang, L., Hetzel, J., Dangl, J.L., and Chory, J. (2014). The growth-defense pivot: crisis management in plants mediated by LRR-RK surface receptors. Trends Biochem. Sci. *39*, 447–456.

Beyer, M., Nesterov, A., Block, I., König, K., Felgenhauer, T., Fernandez, S., Leibe, K., Torralba, G., Hausmann, M., Trunk, U., et al. (2007). Combinatorial synthesis of peptide arrays onto a microchip. Science *318*, 1888.

Bodenhausen, N., Horton, M.W., and Bergelson, J. (2013). Bacterial communities associated with the leaves and the roots of Arabidopsis thaliana. PLoS One *8*, e56329.

Boutrot, F., and Zipfel, C. (2017). Function, discovery, and exploitation of plant pattern recognition receptors for broad-spectrum disease resistance. Annu. Rev. Phytopathol. *55*, 257–286.

Buscaill, P., Chandrasekar, B., Sanguankiattichai, N., Kourelis, J., Kaschani, F., Thomas, E.L., Morimoto, K., Kaiser, M., Preston, G.M., Ichinose, Y., and van der Hoorn, R.A.L. (2019). Glycosidase and glycan polymorphism control hydrolytic release of immunogenic flagellin peptides. Science *364*, 6436.

Capella-Gutiérrez, S., Silla-Martínez, J.M., and Gabaldón, T. (2009). trimAl: a tool for automated alignment trimming in large-scale phylogenetic analyses. Bioinformatics *25*, 1972–1973.

Cesbron, S., Paulin, J.P., Tharaud, M., Barny, M.A., and Brisset, M.N. (2006). The alternative σ factor HrpL negatively modulates the flagellar system in the phytopathogenic bacterium Erwinia amylovora under hrp-inducing conditions. FEMS Microbiol. Lett. *257*, 221–227.

Chen, P., and Zhang, J. (2020). Antagonistic pleiotropy conceals molecular adaptations in changing environments. Nat. Ecol. Evol. *4*, 461–469.

Chen, T., Nomura, K., Wang, X., Sohrabi, R., Xu, J., Yao, L., Paasch, B.C., Ma, L., Kremer, J., Cheng, Y., et al. (2020). A plant genetic network for preventing dysbiosis in the phyllosphere. Nature *580*, 653–657.

Chesnokova, O., Coutinho, J.B., Khan, I.H., Mikhail, M.S., and Kado, C.I. (1997). Characterization of flagella genes of Agrobacterium tumefaciens, and the effect of a bald strain on virulence. Mol. Microbiol. *23*, 579–590.

Chinchilla, D., Bauer, Z., Regenass, M., Boller, T., and Felix, G. (2006). The Arabidopsis receptor kinase FLS2 binds flg22 and determines the specificity of flagellin perception. Plant Cell *18*, 465–476.

Chinchilla, D., Zipfel, C., Robatzek, S., Kemmerling, B., Nürnberger, T., Jones, J.D., Felix, G., and Boller, T. (2007). A flagellin-induced complex of the receptor FLS2 and BAK1 initiates plant defence. Nature *448*, 497–500.

Clarke, C.R., Chinchilla, D., Hind, S.R., Taguchi, F., Miki, R., Ichinose, Y., Martin, G.B., Leman, S., Felix, G., and Vinatzer, B.A. (2013). Allelic variation in two distinct Pseudomonas syringae flagellin epitopes modulates the strength of plant immune responses but not bacterial motility. New Phytol. *200*, 847–860.

Colaianni, N., Parys, K., Lee, H.S., Conway, J.M., Kim, N.H., Edelbacher, N., Mucyn, T.S., Madalinski, M., Law, T.F., Jones, C.D., et al. (2021). A complex immune response to flagellin epitope variation in commensal communities. Cell Host Microbe *29*.

Crooks, G.E., Hon, G., Chandonia, J.M., and Brenner, S.E. (2004). WebLogo: a sequence logo generator. Genome Res. *14*, 1188–1190.

Cull, M.G., and Schatz, P.J. (2000). Biotinylation of proteins in vivo and in vitro using small peptide tags. Methods Enzymol. *326*, 430–440.

Dangl, J.L., Horvath, D.M., and Staskawicz, B.J. (2013). Pivoting the plant immune system from dissection to deployment. Science *341*, 746–751.

Delmotte, N., Knief, C., Chaffron, S., Innerebner, G., Roschitzki, B., Schlapbach, R., von Mering, C., and Vorholt, J.A. (2009). Community proteogenomics reveals insights into the physiology of phyllosphere bacteria. Proc. Natl. Acad. Sci. USA *106*, 16428–16433.

Edgar, R.C. (2004). MUSCLE: multiple sequence alignment with high accuracy and high throughput. Nucleic Acids Res. *32*, 1792–1797.

Fairhead, M., and Howarth, M. (2015). Site-specific biotinylation of purified proteins using BirA. Methods Mol. Biol. *1266*, 171–184.

Felix, G., Duran, J.D., Volko, S., and Boller, T. (1999). Plants have a sensitive perception system for the most conserved domain of bacterial flagellin. Plant J. Cell Mol. Biol. *18*, 265–276.

Fliegmann, J., and Felix, G. (2016). Immunity: flagellin seen from all sides. Nat. Plants *2*, 16136.

Fürst, U., Zeng, Y., Albert, M., Witte, A.K., Fliegmann, J., and Felix, G. (2020). Perception of Agrobacterium tumefaciens flagellin by FLS2XL confers resistance to crown gall disease. Nat. Plants 6, 22–27.

Gibson, D.G., Young, L., Chuang, R.Y., Venter, J.C., Hutchison, C.A., 3rd, and Smith, H.O. (2009). Enzymatic assembly of DNA molecules up to several hundred kilobases. Nat. Methods 6, 343–345.

Gómez-Gómez, L., and Boller, T. (2000). FLS2: an LRR receptor-like kinase involved in the perception of the bacterial elicitor flagellin in Arabidopsis. Mol. Cell 5, 1003–1011.

Gouveia-Oliveira, R., and Pedersen, A.G. (2007). Finding coevolving amino acid residues using row and column weighting of mutual information and multi-dimensional amino acid representation. Algor. Mol. Biol. 2, 12.

Ha, D.G., Kuchma, S.L., and O'Toole, G.A. (2014). Plate-based assay for swarming motility in Pseudomonas aeruginosa. Methods Mol. Biol. 1149, 67–72.

Hacquard, S., Spaepen, S., Garrido-Oter, R., and Schulze-Lefert, P. (2017). Interplay Between innate immunity and the plant microbiota. Annu. Rev. Phytopathol. 55, 565–589.

Hashimoto, Y., Zhang, S., and Blissard, G.W. (2010). Ao38, a new cell line from eggs of the black witch moth, Ascalapha odorata (Lepidoptera: Noctuidae), is permissive for AcMNPV infection and produces high levels of recombinant proteins. BMC Biotechnol. 10, 50.

Hind, S.R., Strickler, S.R., Boyle, P.C., Dunham, D.M., Bao, Z., O'Doherty, I.M., Baccile, J.A., Hoki, J.S., Viox, E.G., Clarke, C.R., et al. (2016). Tomato receptor flagellin-SENSING 3 binds flgII-28 and activates the plant immune system. Nat. Plants 2, 16128.

Hmelo, L.R., Borlee, B.R., Almblad, H., Love, M.E., Randall, T.E., Tseng, B.S., Lin, C., Irie, Y., Storek, K.M., Yang, J.J., et al. (2015). Precision-engineering the Pseudomonas aeruginosa genome with two-step allelic exchange. Nat. Protoc. 10, 1820–1841.

Hohmann, U., Lau, K., and Hothorn, M. (2017). The structural basis of ligand perception and signal activation by receptor kinases. Annu. Rev. Plant Biol. 68, 109–137.

Hohmann, U., Santiago, J., Nicolet, J., Olsson, V., Spiga, F.M., Hothorn, L.A., Butenko, M.A., and Hothorn, M. (2018). Mechanistic basis for the activation of plant membrane receptor kinases by SERK-family coreceptors. Proc. Natl. Acad. Sci. USA 115, 3488–3493.

Iwasaki, A., and Medzhitov, R. (2004). Toll-like receptor control of the adaptive immune responses. Nat. Immunol. 5, 987–995.

Iwasaki, A., and Medzhitov, R. (2015). Control of adaptive immunity by the innate immune system. Nat. Immunol. 16, 343–353.

Jaillais, Y., Belkhadir, Y., Balsemão-Pires, E., Dangl, J.L., and Chory, J. (2011). Extracellular leucine-rich repeats as a platform for receptor/coreceptor complex formation. Proc. Natl. Acad. Sci. USA 108, 8503–8507.

Kadota, Y., Sklenar, J., Derbyshire, P., Stransfeld, L., Asai, S., Ntoukakis, V., Jones, J.D., Shirasu, K., Menke, F., Jones, A., and Zipfel, C. (2014). Direct regulation of the NADPH oxidase RBOHD by the PRR-associated kinase BIK1 during plant immunity. Mol. Cell 54, 43–55.

Kappal, S. (2019). Data normalization using median & median absolute deviation (MMAD) based Z-score for robust predictions vs. min-max normalization.

Karasov, T.L., Almario, J., Friedemann, C., Ding, W., Giolai, M., Heavens, D., Kersten, S., Lundberg, D.S., Neumann, M., Regalado, J., et al. (2018). Arabidopsis thaliana and Pseudomonas pathogens exhibit stable associations over evolutionary timescales. Cell Host Microbe 24, 168–179.e4.

King, E.O., Ward, M.K., and Raney, D.E. (1954). Two simple media for the demonstration of pyocyanin and fluorescin. J. Lab. Clin. Med. 44, 301–307.

Kovach, M.E., Elzer, P.H., Hill, D.S., Robertson, G.T., Farris, M.A., Roop, R.M., 2nd, and Peterson, K.M. (1995). Four new derivatives of the broad-host-range cloning vector pBBR1MCS, carrying different antibiotic-resistance cassettes. Gene 166, 175–176.

Kozma, P., Hamori, A., Cottier, K., Kurunczi, S., and Horvath, R. (2009). Grating coupled interferometry for optical sensing. Appl. Phys. B 97, 5–8.

Kumar, S., Stecher, G., and Tamura, K. (2016). MEGA7: molecular evolutionary genetics analysis version 7.0 for bigger datasets. Mol. Biol. Evol. 33, 1870–1874.

Laflamme, B., Dillon, M.M., Martel, A., Almeida, R.N.D., Desveaux, D., and Guttman, D.S. (2020). The pan-genome effector-triggered immunity landscape of a host-pathogen interaction. Science 367, 763–768.

Lampropoulos, A., Sutikovic, Z., Wenzl, C., Maegele, I., Lohmann, J.U., and Forner, J. (2013). GreenGate—a novel, versatile, and efficient cloning system for plant transgenesis. PLoS One 8, e83043.

Lee, H.S., and Belkhadir, Y. (2020). Damage control: cellular logic in the root immune response. Cell Host Microbe 27, 308–310.

Leys, C., Ley, C., Klein, O., Bernard, P., and Licata, L. (2013). Detecting outliers: do not use standard deviation around the mean, use absolute deviation around the median. J. Exp. Soc. Psychol. 49, 764–766.

Liberati, N.T., Urbach, J.M., Miyata, S., Lee, D.G., Drenkard, E., Wu, G., Villanueva, J., Wei, T., and Ausubel, F.M. (2006). An ordered, nonredundant library of Pseudomonas aeruginosa strain PA14 transposon insertion mutants. Proc. Natl. Acad. Sci. USA 103, 2833–2838.

Lozano-Durán, R., and Belkhadir, Y. (2017). A technical framework for studying the signaling nexus of brassinosteroids and immunity. Methods Mol. Biol. 1564, 49–61.

Lu, D., Wu, S., Gao, X., Zhang, Y., Shan, L., and He, P. (2010). A receptor-like cytoplasmic kinase, BIK1, associates with a flagellin receptor complex to initiate plant innate immunity. Proc Natl Acad Sci U S A 107, 496–501.

Macnab, R.M. (2003). How bacteria assemble flagella. Annu. Rev. Microbiol. 57, 77–100.

McCann, H.C., Nahal, H., Thakur, S., and Guttman, D.S. (2012). Identification of innate immunity elicitors using molecular signatures of natural selection. Proc. Natl. Acad. Sci. USA 109, 4215–4220.

Meindl, T., Boller, T., and Felix, G. (2000). The bacterial elicitor flagellin activates its receptor in tomato cells according to the address-message concept. Plant Cell 12, 1783–1794.

Millet, Y.A., Danna, C.H., Clay, N.K., Songnuan, W., Simon, M.D., Werck-Reichhart, D., and Ausubel, F.M. (2010). Innate immune responses activated in Arabidopsis roots by microbe-associated molecular patterns. Plant Cell 22, 973–990.

Mott, G.A., Thakur, S., Smakowska, E., Wang, P.W., Belkhadir, Y., Desveaux, D., and Guttman, D.S. (2016). Genomic screens identify a new phytobacterial microbe-associated molecular pattern and the cognate Arabidopsis receptor-like kinase that mediates its immune elicitation. Genome Biol. 17, 98.

Naito, K., Taguchi, F., Suzuki, T., Inagaki, Y., Toyoda, K., Shiraishi, T., and Ichinose, Y. (2008). Amino acid sequence of bacterial microbe-associated molecular pattern flg22 is required for virulence. Mol. Plant Microbe Interact. 21, 1165–1174.

Nekrasov, V., Li, J., Batoux, M., Roux, M., Chu, Z.H., Lacombe, S., Rougon, A., Bittel, P., Kiss-Papp, M., Chinchilla, D., et al. (2009). Control of the pattern-recognition receptor EFR by an ER protein complex in plant immunity. EMBO J. 28, 3428–3438.

Okuda, S., Fujita, S., Moretti, A., Hohmann, U., Doblas, V.G., Ma, Y., Pfister, A., Brandt, B., Geldner, N., and Hothorn, M. (2020). Molecular mechanism for the recognition of sequence-divergent CIF peptides by the plant receptor kinases GSO1/SGN3 and GSO2. Proc. Natl. Acad. Sci. USA 117, 2693–2703.

Pel, M.J.C., van Dijken, A.J.H., Bardoel, B.W., Seidl, M.F., van der Ent, S., van Strijp, J.A.G., and Pieterse, C.M.J. (2014). Pseudomonas syringae evades host immunity by degrading flagellin monomers with alkaline protease AprA. Mol. Plant Microbe Interact. 27, 603–610.

Poncini, L., Wyrsch, I., Dénervaud Tendon, V., Vorley, T., Boller, T., Geldner, N., Métraux, J.P., and Lehmann, S. (2017). In roots of Arabidopsis thaliana, the damage-associated molecular pattern AtPep1 is a stronger elicitor of immune signalling than flg22 or the chitin heptamer. PLoS One 12, e0185808.

Ramos, H.C., Rumbo, M., and Sirard, J.C. (2004). Bacterial flagellins: mediators of pathogenicity and host immune responses in mucosa. Trends Microbiol. 12, 509–517.

Rietsch, A., Vallet-Gely, I., Dove, S.L., and Mekalanos, J.J. (2005). ExsE, a secreted regulator of type III secretion genes in Pseudomonas aeruginosa. Proc. Natl. Acad. Sci. USA 102, 8006–8011.

Robatzek, S., Bittel, P., Chinchilla, D., Köchner, P., Felix, G., Shiu, S.H., and Boller, T. (2007). Molecular identification and characterization of the tomato flagellin receptor LeFLS2, an orthologue of Arabidopsis FLS2 exhibiting characteristically different perception specificities. Plant Mol. Biol. 64, 539–547.

Rossez, Y., Wolfson, E.B., Holmes, A., Gally, D.L., and Holden, N.J. (2015). Bacterial flagella: twist and stick, or dodge across the kingdoms. PLoS Pathog. 11, e1004483.

Sambrook, J., Fritsch, E.F., and Maniatis, T. (1989). Molecular Cloning: A Laboratory Manual (Cold Spring Harbor Laboratory Press).

Schindelin, J., Arganda-Carreras, I., Frise, E., Kaynig, V., Longair, M., Pietzsch, T., Preibisch, S., Rueden, C., Saalfeld, S., Schmid, B., et al. (2012). Fiji: an open-source platform for biological-image analysis. Nat. Methods 9, 676–682.

Schneider, C.A., Rasband, W.S., and Eliceiri, K.W. (2012). NIH Image to ImageJ: 25 years of image analysis. Nat. Methods 9, 671–675.

Schulze, B., Mentzel, T., Jehle, A.K., Mueller, K., Beeler, S., Boller, T., Felix, G., and Chinchilla, D. (2010). Rapid heteromerization and phosphorylation of ligand-activated plant transmembrane receptors and their associated kinase BAK1. J. Biol. Chem. 285, 9444–9451.

Sitaraman, R. (2015). Pseudomonas spp. as models for plant-microbe interactions. Front. Plant Sci. 6, 787.

Smakowska, E., Kong, J., Busch, W., and Belkhadir, Y. (2016). Organ-specific regulation of growth-defense tradeoffs by plants. Curr. Opin. Plant Biol. 29, 129–137.

Smakowska-Luzan, E., Mott, G.A., Parys, K., Stegmann, M., Howton, T.C., Layeghifard, M., Neuhold, J., Lehner, A., Kong, J., Grünwald, K., et al. (2018). An extracellular network of Arabidopsis leucine-rich repeat receptor kinases. Nature 553, 342–346.

Stadler, V., Felgenhauer, T., Beyer, M., Fernandez, S., Leibe, K., Güttler, S., Gröning, M., König, K., Torralba, G., Hausmann, M., et al. (2008). Combinatorial synthesis of peptide arrays with a laser printer. Angew. Chem. Int. Ed. Engl. 47, 7132–7135.

Sun, W., Dunning, F.M., Pfund, C., Weingarten, R., and Bent, A.F. (2006). Within-species flagellin polymorphism in Xanthomonas campestris pv campestris and its impact on elicitation of Arabidopsis flagellin SENSING2-dependent defenses. Plant Cell 18, 764–779.

Sun, Y., Li, L., Macho, A.P., Han, Z., Hu, Z., Zipfel, C., Zhou, J.M., and Chai, J. (2013). Structural basis for flg22-induced activation of the Arabidopsis FLS2-BAK1 immune complex. Science 342, 624–628.

Taguchi, F., Yamamoto, M., Ohnishi-Kameyama, M., Iwaki, M., Yoshida, M., Ishii, T., Konishi, T., and Ichinose, Y. (2010). Defects in flagellin glycosylation affect the virulence of Pseudomonas syringae pv. tabaci 6605. Microbiol. Reading Engl. 156, 72–80.

Takai, R., Isogai, A., Takayama, S., and Che, F.S. (2008). Analysis of flagellin perception mediated by flg22 receptor OsFLS2 in rice. Mol. Plant Microbe Interact. 21, 1635–1642.

Teixeira, P.J.P.L., Colaianni, N.R., Fitzpatrick, C.R., and Dangl, J.L. (2019). Beyond pathogens: microbiota interactions with the plant immune system. Curr. Opin. Microbiol. 49, 7–17.

Trdá, L., Fernandez, O., Boutrot, F., Héloir, M.C., Kelloniemi, J., Daire, X., Adrian, M., Clément, C., Zipfel, C., Dorey, S., and Poinssot, B. (2014). The grapevine flagellin receptor VvFLS2 differentially recognizes flagellin-derived epitopes from the endophytic growth-promoting bacterium Burkholderia phytofirmans and plant pathogenic bacteria. New Phytol. 201, 1371–1384.

Venkataram, S., Monasky, R., Sikaroodi, S.H., Kryazhimskiy, S., and Kacar, B. (2020). Evolutionary stalling and a limit on the power of natural selection to improve a cellular module. Proc. Natl. Acad. Sci. USA 117, 18582–18590.

Vetter, M., Karasov, T.L., and Bergelson, J. (2016). Differentiation between MAMP triggered defenses in Arabidopsis thaliana. PLoS Genet. 12, e1006068.

Wang, F., Burrage, A.M., Postel, S., Clark, R.E., Orlova, A., Sundberg, E.J., Kearns, D.B., and Egelman, E.H. (2017). A structural model of flagellar filament switching across multiple bacterial species. Nat. Commun. 8, 960.

Wang, J., Grubb, L.E., Wang, J., Liang, X., Li, L., Gao, C., Ma, M., Feng, F., Li, M., Li, L., et al. (2018). A regulatory module controlling homeostasis of a plant immune kinase. Mol. Cell 69, 493–504.e6.

Wang, S., Sun, Z., Wang, H., Liu, L., Lu, F., Yang, J., Zhang, M., Zhang, S., Guo, Z., Bent, A.F., and Sun, W. (2015). Rice OsFLS2-Mediated Perception of Bacterial Flagellins Is Evaded by Xanthomonas oryzae pvs. oryzae and oryzicola. Mol. Plant 8, 1024–1037.

Wei, Y., Balaceanu, A., Rufian, J.S., Segonzac, C., Zhao, A., Morcillo, R.J.L., and Macho, A.P. (2020). An immune receptor complex evolved in soybean to perceive a polymorphic bacterial flagellin. Nat. Commun. 11, 3763.

Whelan, S., and Goldman, N. (2001). A general empirical model of protein evolution derived from multiple protein families using a maximum-likelihood approach. Mol. Biol. Evol. 18, 691–699.

Winsor, G.L., Griffiths, E.J., Lo, R., Dhillon, B.K., Shay, J.A., and Brinkman, F.S. (2016). Enhanced annotations and features for comparing thousands of Pseudomonas genomes in the Pseudomonas genome database. Nucleic Acids Res. 44, D646–D653.

Wyrsch, I., Domínguez-Ferreras, A., Geldner, N., and Boller, T. (2015). Tissue-specific FLAGELLIN-SENSING 2 (FLS2) expression in roots restores immune responses in Arabidopsis fls2 mutants. New Phytol. 206, 774–784.

Yonekura, K., Maki-Yonekura, S., and Namba, K. (2003). Complete atomic model of the bacterial flagellar filament by electron cryomicroscopy. Nature 424, 643–650.

Yoon, S.I., Kurnasov, O., Natarajan, V., Hong, M., Gudkov, A.V., Osterman, A.L., and Wilson, I.A. (2012). Structural basis of TLR5-flagellin recognition and signaling. Science 335, 859–864.

Zhou, F., Emonet, A., Dénervaud Tendon, V., Marhavy, P., Wu, D., Lahaye, T., and Geldner, N. (2020). Co-incidence of damage and microbial patterns controls localized immune responses in roots. Cell 180, 440–453.e18.

Zipfel, C., Robatzek, S., Navarro, L., Oakeley, E.J., Jones, J.D., Felix, G., and Boller, T. (2004). Bacterial disease resistance in Arabidopsis through flagellin perception. Nature 428, 764–767.

STAR★METHODS

KEY RESOURCES TABLE

REAGENT or RESOURCE	SOURCE	IDENTIFIER
Antibodies		
Mouse monoclonal anti-Flagellin FliC	InvivoGen	Cat# mabg-flapa removed from catalog since 01/20/2020
Mouse monoclonal anti-Flag-HRP	Sigma Aldrich	Cat#A8592; RRID: AB_439702
Rabbit polyclonal anti-BAK1	Agrisera	Cat#AS121858; RRID: AB_2884902
Mouse monoclonal anti-HA-HRP	Miltenyi Biotec	Cat# 130-091-972; RRID: AB_871936
Rabbit polyclonal anti-GFP-HRP	Sigma Aldrich	Cat# A10260; RRID: AB_2534022
Mouse monoclonal anti-V5-HRP	Sigma Aldrich	Cat# R961-25; RRID: AB_2556565
Rabbit polyclonal anti-Mouse-HRP	Sigma Aldrich	Cat# A9044; RRID: AB_258431
Goat polyclonal anti-Rabbit-HRP	Sigma Aldrich	Cat# A6154; RRID: AB_258284
Bacterial and virus strains		
Pseudomonas aeruginosa PA14	Udo Bläsi laboratory	N/A
Pseudomonas aeruginosa PA14 *ΔfliC*	This paper	N/A
Pseudomonas aeruginosa PA14 *ΔfliC-fliC*[x]	This paper	See Table S2
Pseudomonas syringae pv. *tomato* DC3000 *ΔfliC*	Cyril Zipfel laboratory	N/A
Pseudomonas syringae pv. *tomato* DC3000 *ΔfliC-fliC*[Ps flg22]	This paper	N/A
Pseudomonas syringae pv. *tomato* DC3000 *ΔfliC-fliC*[Pa flg22]	This paper	N/A
Pseudomonas syringae pv. *tomato* DC3000 *ΔfliC*-EV	This paper	N/A
Pseudomonas syringae pv. *tomato* DC3000 *ΔfliC-fliC*[Pa flg22-D14K]	This paper	N/A
Pseudomonas syringae pv. *tomato* DC3000 *ΔfliC-fliC*[Pa flg22-D15K]	This paper	N/A
Pseudomonas syringae pv. *tomato* DC3000 *ΔfliC-fliC*[Pa flg22-I21D]	This paper	N/A
Pseudomonas syringae pv. *tomato* DC3000 *ΔfliC-fliC*[Pa flg22-Q20D]	This paper	N/A
Pseudomonas syringae pv. *tomato* DC3000 *ΔfliC-fliC*[Pa flg22-G18F]	This paper	N/A
Pseudomonas syringae pv. *tomato* DC3000 *ΔfliC-fliC*[Pa flg22-I21E]	This paper	N/A
Pseudomonas syringae pv. *tomato* DC3000 *ΔfliC-fliC*[Pa flg22-A16D]	This paper	N/A
Pseudomonas syringae pv. *tomato* DC3000 *ΔfliC-fliC*[Pa flg22-K13D]	This paper	N/A
Pseudomonas syringae pv. *tomato* DC3000 *ΔfliC-fliC*[Pa flg22-S11D]	This paper	N/A
Pseudomonas syringae pv. *tomato* DC3000 *ΔfliC-fliC*[Pa flg22-A22D]	This paper	N/A
Pseudomonas syringae pv. *tomato* DC3000 *ΔfliC-fliC*[Pa flg22-K13Y]	This paper	N/A
Pseudomonas syringae pv. *tomato* DC3000 *ΔfliC-fliC*[Pa flg22-A22E]	This paper	N/A
Pseudomonas syringae pv. *tomato* DC3000 *ΔfliC-fliC*[Pa flg22-chGDG]	This paper	N/A
Pseudomonas syringae pv. *tomato* DC3000 *ΔfliC-fliC*[Pa flg22-GDG]	This paper	N/A
Pseudomonas syringae pv. *tomato* DC3000 *ΔfliC-fliC*[Pa flg22-chNSS]	This paper	N/A
Pseudomonas syringae pv. *tomato* DC3000 *ΔfliC-fliC*[Pa flg22-NSS]	This paper	N/A
NEB 10-beta Competent *Escherichia coli*	New England BioLabs	Cat#C3019I
Chemicals, peptides, and recombinant proteins		
Murashige & Skoog salt + Gamborg B5 Vit.	Duchefa	Cat#M0231.0050
Agar Bacteriology grade	PlanReac AppliChem ITW Reagents	Cat#A0949,0500, CAS: 9002-18-0
EDTA-free protein inhibitor cocktail	Roche	Cat#45-5056489001
Luminol	Sigma-Aldrich	Cat#A8511, CAS: 521-31-3
L-012Luminol	Wako Chemicals USA	Cat#NC0733364
Horse Radish Peroxidase	ThermoFisher Scientific	Cat#31490, CAS: 9003-99-0
ExpreS[2] Insect-TRx5 Transfection Reagent	Expression System	Cat#S2-55A-001

(Continued on next page)

Continued

REAGENT or RESOURCE	SOURCE	IDENTIFIER
KPL BluePhos Microwell Phosphatase Substrate System	Sera care	Cat#5120-0059
Human recombinant IgG1-Fc protein	ThermoFisher Scientific	Cat#A42558
Phusion High-Fidelity DNA Polymerase	ThermoFisher Scientific	Cat#F530S
Phusion Flash High-Fidelity DNA Polymerase	ThermoFisher Scientific	Cat#F548S
FastDigest DpnI	ThermoFisher Scientific	Cat#FD1704
GFP-Trap A beads	Chromotek	Cat#gta-100
HisTrap excel	GE Healthcare	Cat#17371205
Strep-Tactin Superflow high capacity	IBA	Cat#: 2-1208-500
Flg22 peptides	This paper – in-house Protein Chemistry Facility and Shanghai Apeptide Co.	N/A
Extracellular domain (ECD) of FLS2^{LRR} - StrepII-6xHis	This paper	N/A
FLS2$^{1-800}$ -Avi -TEV - StrepII-9xHis tag	Michael Hothorn laboratory, Okuda et al., 2020	N/A
BAK1$^{1-220}$ –TEV - StrepII - 9xHis tag	Michael Hothorn laboratory, Hohmann et al.. 2018	N/A
FLS2^{LRR} – Fc-V5 ECD	Smakowska-Luzan et al., 2018	RRID:Addgene_115120
BAK1^{LRR} – AP-Flag ECD	Smakowska-Luzan et al., 2018	RRID:Addgene_114775
Critical commercial assays		
Custom flg22 peptide array	PepperPrint	N/A
Wizard SV Gel and PCR Clean-Up system	Promega	Cat#A9281
4PCP WAVEchip	Creoptix AG	N/A
Deposited data		
528 *Pseudomonads* flg22 sequences parsed from the Pseudomonas database (Winsor et al., 2016)	This paper	See Table S1
1490 flg22 sequences found in *Ps* OTUs isolates and parsed from Karasov et al., 2018	This paper	See Table S4
Snprator.r R script	This paper	https://github.com/arthurkorte/SNP_extractor
Raw results obtained for flg22 peptides interrogations with FLS2^{ECD} derived from the mutational scan of Pa flg22	This paper	https://doi.org/10.17632/ccvvsv8g3w.1
Raw swimming motility results for *Pseudomonas aeruginosa* PA14 mutational compendium	This paper	https://doi.org/10.17632/ccvvsv8g3w.1
Experimental models: cell lines		
Trichoplusia ni strain High Five cells	Protein Technologies Facility of the Vienna Biocenter Core Facilities	Expression Systems; 94-002F
Trichoplusia ni strain Tnao38 cells	Hashimoto et al., 2010	RRID: CVCL_Z252
Drosophila melanogaster Schneider 2 (S2) cells	Protein Technologies Facility of the Vienna Biocenter Core Facilities	Expression Systems; 94-005F
Experimental models: organisms/strains		
Arabidopsis thaliana Col-0	Youssef Belkhadir lab stock	NCBI: txid3702
Arabidopsis: *proFLS2:FLS2-GFP*	Chinchilla et al., 2007	*fls2* mutant
Arabidopsis: fls2 efr	Nekrasov et al., 2009	SAIL_691_C4 / Salk_044334
Arabidopsis: *proMYB51:NLS-3mVenus*	Poncini et al., 2017	Transgenic Col-0
Arabidopsis: *proWRKY11:NLS-3mVenus*	Poncini et al., 2017	Transgenic Col-0
Arabidopsis: *proCYP71A12:GUS*	Millet et al., 2010	Transgenic Col-0
Arabidopsis: *proBIK1:BIK1-HA*	Kadota et al., 2014	Transgenic Col-0

Continued

REAGENT or RESOURCE	SOURCE	IDENTIFIER
Oligonucleotides		
DNA primers	Sigma Aldrich	See Table S7
fliC mutational compendium gene synthesis and custom cloning	Genewiz	See Table S2
Recombinant DNA		
Suicide vector pEXG2	Rietsch et al., 2005; Udo Bläsi	N/A
Broad-host-range vector pBBR1-MSC5	Kovach et al., 1995; Jeff Chang laboratory	N/A
Broad-host-range vector pGGrhizo_Plum	This paper; Claude Becker laboratory	N/A
pMel Bac B1 - FLS2^{LRR} - StrepII-6xHis ECD	This paper	N/A
pFastBac- FLS2$^{1-800}$ -Avi -TEV - StrepII-9xHis tag	Geneva Biotech/ (Okuda et al., 2020)	GVA-UH367
pFastBac- BAK1$^{1-220}$ –TEV - StrepII - 9xHis tag	Geneva Biotech/ (Hohmann et al., 2018)	GVA-UH147
pECIA-2-FLS2^{LRR} ECD	Smakowska-Luzan et al., 2018	RRID:Addgene_115120
pECIA-14-BAK1^{LRR} ECD	Smakowska-Luzan et al., 2018	RRID:Addgene_114775
Software and algorithms		
R language and software environment (version R 3.6.1)	R Core Team (2019)	https://www.r-project.org; RRID:SCR_001905
GraphPad Prism 8.0	GraphPad Software	https://www.graphpad.com; RRID:SCR_002798
Image J	Schneider et al., 2012	https://imagej.nih.gov/ij/; RRID:SCR_003070
Fiji	Schindelin et al., 2012	https://imagej.net/Fiji RRID:SCR_002285
PyMOL v1.6.0.0.	The PyMOL Molecular Graphics System, Version 1.6.0.0. Schrödinger, LLC.	https://pymol.org/2/; RRID:SCR_000305
WebLOGO	(Crooks et al., 2004)	https://weblogo.berkeley.edu/logo.cgi; RRID:SCR_010236
Mutual Information Theory (MIT)	Gouveia-Oliveira and Pedersen, 2007	https://github.com/ncolaian/flagellin_antag_pleiotropy
MEGA7	Kumar et al., 2016	https://www.megasoftware.net/
SPOT 5.1	SPOT imaging	N/A
WAVEcontrol	Creoptix	N/A
RainCloud Code used for Figure 1B and Figure 3A visualization	Allen et al., 2019	https://github.com/RainCloudPlots/RainCloudPlots.
Other		
μ-Slide VI0.4	Ibidi	Cat#80606

RESOURCE AVAILABILITY

Lead contact
Further information and requests for resources and reagents should be directed to and will be fulfilled by the Lead Contact, Youssef Belkhadir (youssef.belkhadir@gmi.oeaw.ac.at).

Materials availability
Plasmids and bacterial strains generated in this study will be made available on request, but we may require a completed Materials Transfer Agreement if there is potential for commercial application.

Data and code availability

All the original/source data are available on Mendeley Data (https://doi.org/10.17632/ccvvsv8g3w.1). The data for the flg22 peptide array and Pseudomonas mutation scans for bacterial swimming motility are additionally available at: https://github.com/kateparys/Parys-et-al.-2021. The codes and raw data for Mutual Information Theory is available at https://github.com/ncolaian/flagellin_antag_pleiotropy.

EXPERIMENTAL MODEL AND SUBJECT DETAILS

Plant material and growth conditions

Arabidopsis thaliana accession Columbia (Col-0) was used as wild type in all experiments performed. The mutant line *fls2 efr* (SAIL_691_C4 / Salk_044334) was described elsewhere (Nekrasov et al., 2009). The transgenic lines *proFLS2:FLS2-GFP* (Chinchilla et al., 2007), *proMYB51:NLS-3mVenus, proWRKY11:NLS-3mVenus*, *proCYP71A12:GUS* (Poncini et al., 2017), and *proBIK1:BIK1-HA* (Kadota et al., 2014) were described previously. Plants were grown on soil in short-day light conditions (12 h light/12 h dark) or vertically in Petri dishes containing 1/2 Murashige and Skoog (MS) medium (Duchefa), 0.8% plant agar (ITW reagents), and 1% sucrose in long-day light conditions (16 h light/8 h dark).

Bacterial strains

All bacterial strains are listed in the key resources table and Table S2.

METHODS DETAILS

Presentation of the data in the main figures

Figure 1: B, at least 8 independent replicates per allelic variant were used for the analysis of *Pa* swimming motility. Figure 4: A and C, the box plots represent the first and third quartiles, centered by the median. Whiskers include the 10th–90th percentile of the data points. Dots represent individual observations from either three (A) or two (C) independent experiments. Figure 5: A–D, the box plots represent the first and third quartiles, centered by the median. Whiskers include the 10th–90th percentile of the data. Dots represent individual observations from either three (A, B and C) or two (D) independent experiments. Figure 5C Pa flg22 peptide was used as a control sample and comparator for statistical analysis. E, the bar plot shows the percentages of sick leaves scored on 8 rosettes from two independent experiments. The error bars indicate the standard error from at these two biological repetitions. Figure 6: B, the Co-IP assays were repeated three times with similar results. C, the error bars on the plots indicate the standard deviation from at least two biological repetitions. D, the Co-IP assays were repeated two times with similar results. Figure 7: B, C, and F, the box plot represents the first and third quartiles, centered by the median. Whiskers include the 10th-90th percentile of the data points from at least two independent biological experiments. D and E: the Co-IP assays were repeated two times with similar results. Information about data and replication is included in all the legends of supplemental figures.

Deletion of *fliC* from *Pseudomonas aeruginosa* (*Pa*) PA14

To construct an in-frame deletion of *fliC*, two PCR products flanking the *fliC* gene were obtained from *Pa* PA14 chromosomal DNA by PCR amplification with primer pairs O183/P183 and Q183/R183 (Table S7) (Liberati et al., 2006). The combined 729-bp upstream and 723-bp downstream fragments were used as a template for a second overlapping PCR with primers O183 and R183, because primers P183 and Q183 contained a complementary sequence. The resulting fragment, a 1464-bp deletion spanning the entire *fliC* coding region except for the stop codon (coordinates 4465410-4466873 of the *Pa* PA14 genome (Winsor et al., 2016)), was digested with BamHI and KpnI and ligated into the corresponding sites of the suicide vector pEXG2 (Rietsch et al., 2005), resulting in plasmid pEXG2-Δ*fliC*. All DNA manipulations were verified by DNA sequencing. The strain *Pa* PA14 *ΔfliC* was constructed by homologue recombination. Briefly, plasmid pEXG2-Δ*fliC* was mobilized into the strains *Pa* PA14 with the aid of *E. coli* strain S17-1, and then chromosomally integrated through selection for gentamicin. Excision of the vector by a second crossover was achieved by selection of sucrose insensitive cells as the pEXG2 vector encodes the *Bacillus subtilis* sacB gene, whose gene product - levansucrase - renders Gram-negative cells sensitive to sucrose (Hmelo et al., 2015; Rietsch et al., 2005).

Cloning of allelic variants of *Pa fliC* gene and complementation *of Pa ΔfliC*

Pa fliC gene (NZ_JTUE01000011.1) was designed to comprise the FliC coding sequence and regions 405 bp upstream of the start codon and 78 bp downstream of the stop codon. Upon gene synthesis (Genewiz®), the *fliC* genes were cloned into the modified broad-host-range vector pBBR1-MSC5 (Kovach et al., 1995) using the BstBI and NsiI restriction sites. The mutant library of 412 *fliC* allelic variants was constructed using the same method. The resulting pBBR1-MSC5-*fliC*' plasmids were verified by DNA sequencing and introduced into *Pa ΔfliC* via conjugation. Briefly, overnight liquid cultures of the *E. coli* helper strain pRK2013, *Pa ΔfliC*, and *E.coli* transformed with pBBR1-MSC5-*fliC*' plasmids were mixed in a ratio 1:1:1 and spotted on a Luria broth (LB) plates (Sambrook et al., 1989). The next day, positive transformants were selected on LB supplemented with gentamycin [25 μg/ml] and chloramphenicol [10 μg/ml]. Positive transformants were verified by colony PCR using the fliC_pBBR1-MSC5_FP and fliC_pBBR1-MSC5_RP primers (Table S7). 20 randomly selected transformants were subjected to Sanger sequencing for verification of inserts.

Quantification of bacterial motility in swim plate assay

Pa Δ*fliC* strains were grown overnight on LB agar plates supplemented with appropriate antibiotics at 37°C. The next day, fresh swim plates were prepared with M9 Minimal media supplemented with 0.3% agar (Ha et al., 2014; Sambrook et al., 1989). The plates were then tooth-pick inoculated with a sterile 2 μl pipette tip by placing the tip in an overnight culture and then onto the swim plate. Pictures of the plates were acquired 24 h after inoculation. The diameter (d) of the bacterial halo was measured in Image J and the halo area was calculated using the formula $(\pi/4) \times d^2$ (Schneider et al., 2012). To confirm the expression of flagellin in *P. aeruginosa fliC* allelic clones with reduced or no motility, we performed Western Blot analysis using Anti-flagellin antibodies (InvivoGen) and anti-Mouse-HRP antibodies (Sigma Aldrich) (Figure S1B). The molecular shift of the band corresponding to flagellin (Figure S1B) may be caused by different flagellin glycosylation patterns and/or other posttranslational modifications. The swimming motility assay for *Pseudomonas syringae* pv *tomato* DC3000 *(Ps)* Δ*fliC* mutants was performed as previously described (Clarke et al., 2013). Briefly, the bacteria were toothpick inoculated on freshly prepared 0.25% agar plates containing King's B medium (KB) supplemented with appropriate antibiotics (King et al., 1954). The plates were incubated at 28°C and pictures of bacteria were acquired 48 h after inoculation. The diameter (d) of the bacterial halo was measured in Image J and the halo area was calculated using the formula $(\pi/4) \times d^2$.

FLS2 extracellular domain expression and purification for peptide array interrogation

The extracellular domain (ECD) of FLS2 from *Arabidopsis thaliana* (amino acids 24 - 804) was cloned into the baculovirus transfer vector pMel Bac B1 (Invitrogen). A C-terminal Strep II - 6xHis tag was fused to the ECD. The FLS2^{LRR} - StrepII-6xHis ECD was produced by secreted expression in baculovirus-infected *Trichoplusia ni* High Five insect cells (Expression Systems) and harvested 72 h post-infection. Subsequently, the protein was purified using Ni-NTA chromatography (Ni Sepharose excel, GE Healthcare) and subjected to size-exclusion chromatography (Superdex 200 16/60, GE Healthcare) in buffer containing 10 mM Bis-Tris pH 6.0, 100 mM NaCl. The protein was concentrated to ~ 3.0 mg/ml.

High-density peptide array design and analysis of interaction scores

The peptide microarrays were made by and purchased from PepperPrint® (Beyer et al., 2007; Stadler et al., 2008). The custom arrays were designed to comprise single amino acid mutational scans of both the full-length Pa flg22 peptide (QRLSTGSRINSAKDDAAGLQIA) and epitope variants truncated at either or both of the N- and C-terminal moieties through a stepwise deletion series from both extremities of Pa flg22 (Figure S2A). All flg22 peptides were printed at least in duplicate, while the non-mutated reference variants were printed 23 times on the array. Overall, 3,268 flg22 peptides were interrogated with the purified FLS2^{ECD} at pH 6 and with a protein concentration of 20 μg/ml, followed by staining with the secondary anti-6xHis Epitope Tag DyLight 680 antibody. HA and Flag control peptides framed the array and served as an internal quality control. The on-array FLS2-flg22 interactions were quantified using LI-COR Odyssey Imaging System, based on the 16-bit gray scale tiff files at scanning intensities of 7/7 and the microarray image analysis was performed using PepSlide® Analyzer. Given that different signal intensities were observed for the different peptide lengths, the data were categorized into four subgroups (Figure S2A). To calculate the interaction score, the raw median intensities for each peptide were Log$_2$ transformed to ensure symmetric distribution of the data. To assess the internal consistency of the flg22 array data, correlation between the three sectors of the full-length substitution scan of flg22 was calculated using Spearman's correlation coefficient (r ~ 0.7 - 0.9). Next, we applied a Median Absolute Deviation (MAD) scale normalization to calculate the interaction scores, where the unmutated variant of the flg22 derivative for each category was established as a reference sample for a respective dataset (Kappal, 2019; Leys et al., 2013). The residuals from the non-mutated Pa flg22 (or truncated variants, respectively) printed at random at least 23 times were used to calculate the median MAD for each subgroup. Subsequently, modified Z-scores for FLS2^{ECD} interactions were calculated for each array spot using their respective non-mutated flg22 variant's median and median absolute deviation with a formula: Z-score = (Log$_2$ median intensity$^{flg22' peptide}$ - Log$_2$ median intensity$^{Pa flg22}$)/MAD$^{Pa flg22}$. We then calculated the median Z-score for each individual peptide variant, hereafter referred to as the interaction score. To understand the variability between interaction scores for peptides derived from the full-length Pa flg22 substitution scan, we applied descriptive statistics. Flg22 peptides with an interaction score above or below the canonical Pa flg22 interquartile region (IQR) were assigned as variants with strong/weak on-chip interaction with FLS2^{ECD}. Variants that reside outside of the 1.5*IQR of Pa flg22 (interaction score >3.12 and <−2.86, respectively) were considered to be significant on-chip FLS2^{ECD} binders/non-binders for the purpose of functional validation of the peptide array data.

Design and cloning of GreenGate compatible, fluorophore tagged broad host range vector

To quantify the motility of *Ps* Δ*fliC* strains, we generated the vector pGGrhizo_Plum. pGGrhizo_Plum was designed to be compatible with modules for the green-gate modular cloning toolkit (Lampropoulos et al., 2013) and thus uses the same sticky-end overhangs as green-gate modules A-F. In contrast to green-gate, there is no resistance cassette module (module G), because the vector backbone carries a gentamycin resistance gene (*gmR*). The green-gate acceptor module was cloned from pGGZ002 using primers 13 and 14 (Table S7). The Plum expresses mPlum fluorescent protein (primers 13-18), driven by *lacP*. The mPlum, replication origins and resistance cassettes were amplified from rainbow vectors (Barbier and Damron, 2016) and assembled with the greengate cloning site using Gibson assembly (Gibson et al., 2009). Inserts were verified by sanger sequencing using primers 21 and 22 (Table S7).

Cloning and complementation of *Ps fliC*

The *Ps fliC* gene, including its promoter and terminator regions (Clarke et al., 2013), was PCR amplified from genomic DNA using Phusion High-Fidelity DNA Polymerase (Thermo Scientific, Cat. No. F530S) and primers fliC_Ps.syr_GreenGate FP/RP (Table S7). To generate the empty vector (EV) control, primers fliC_Ps.syr_GreenGate FP and fliC_Ps.syr_GreenGate_EV were used. The PCR products were separated via gel electrophoresis and purified using the Wizard® SV Gel and PCR Clean-Up System (Promega). The insert was cloned into the broad-host-range pGGrhizo_Plum vector using Gibson assembly. Correct clones were verified by colony PCR and Sanger sequencing using primers listed in Table S7. Mutations (single or multiple) within the flg22 segment of the *fliC* gene were introduced via PCR-based site-directed mutagenesis using Phusion Flash High-Fidelity polymerase (Thermo Scientific, Cat. No. F548S) and primers listed in Table S7. The PCR products were separated via gel electrophoresis, purified from agarose gel, subjected to restriction digest with FastDigest DpnI restriction enzyme (Thermo Scientific, Cat. No. FD1704) and transformed into NEB 10-beta competent *E. coli* (NEB, Cat. No. C3019I). The resulting pGGrhizo_Plum -fliC' plasmids were verified by DNA sequencing and introduced into *Ps ΔfliC* via conjugation as described above. Positive transformants were selected on KB agar plates supplemented with gentamycin [25 μg/ml], chloramphenicol [25 μg/ml] and rifampicin [25 μg/ml] and verified by colony PCR using fliC_syr_FP_339 and Ps.syr-qPCR_RP primers (Table S7).

Microscopic observation of bacterial motility in liquid media

Liquid cultures of *Ps ΔfliC* strains grown overnight in KB media at 28°C were diluted to 600 nm OD_{600} = 0.15. 15 μl of bacterial suspension was loaded onto μ-Slide VI0.4 (Ibidi, Cat. No. 80606) channels and examined using a Zeiss AXIO Vert A1 with phase contrast filter. Movies recording bacterial movement in liquid media were obtained from 200 images using the SPOT 5.1 software (SPOT imaging).

Expression and purification of $FLS2^{ECD}$ and $BAK1^{ECD}$ for GCI assay

The ECDs of FLS2 (amino acids 1 – 800) and BAK1 (amino acids 1 – 220) were amplified from *A. thaliana* genomic DNA or cDNA and cloned into a modified pFastBac vector (Geneva Biotech), containing a TEV (tobacco etch virus protease) cleavable C-terminal StrepII - 9xHis tag as well as a non-cleavable Avi tag (Cull and Schatz, 2000; Fairhead and Howarth, 2015) for FLS2. *Trichoplusia ni* (strain Tnao38 (Hashimoto et al., 2010)) cells were infected with a multiplicity of infection (MOI) of 1 at a density of $2x10^6$ cells/ml and incubated for 26 h at 28°C and 48 h at 22°C. The secreted protein was purified using Ni-NTA (HisTrap excel;GE Healthcare; equilibrated in 25 mM KP_i pH 7.8, 500 mM NaCl) and StrepII (Strep-Tactin Superflow high capacity; IBA; equilibrated in 25 mM Tris pH 8.0, 250 mM NaCl, 1 mM EDTA) affinity chromatography. The StrepII – 9xHis tag was cleaved by incubation with a His tagged TEV protease at 4°C and removed through a second Ni^{2+} affinity chromatography step. Protein purity was further improved by size-exclusion chromatography on a HiLoad 16/600 Superdex 200 column (GE Healthcare), equilibrated in 20 mM sodium citrate pH 5.0, 250 mM NaCl. His-tagged BirA was purified from *E. coli* by Ni^{2+} affinity chromatography.

Biotinylation of $FLS2^{ECD}$

Purified $FLS2^{ECD}$ containing the Avi tag (20 – 100 μM) was incubated with BirA (Fairhead and Howarth, 2015) for 1 h at 25°C in a total volume of 200 μl 25 mM Tris pH 8, 150 mM NaCl, 5 mM $MgCl_2$, 2 mM 2-Mercaptoethanol, 0.15 mM Biotin, 2 mM ATP. BirA as well as free biotin were subsequently separated from the biotinylated FLS2 ectodomain through size-exclusion chromatography.

Peptide synthesis

Pa flg22, flg20 and flg22 peptide derivatives (Data S2) were synthesized by our in-house protein chemistry facility at >95% purity or purchased from Shanghai Apeptide Co. An additional leucine (L) was added to the N terminus of all peptides to avoid conversion of glutamine (Q) to pyroglutamate. The peptides were dissolved in pure water to a final concentration 100 μM, aliquoted, and stored at -20°C. Peptide purity was validated by MALDI-TOF MS (Data S3).

Grating coupled interferometry (GCI)

GCI experiments were performed on a Creoptix WAVE system (Creoptix AG, Switzerland), a label-free surface biosensor (Kozma et al., 2009), using 4PCP WAVEchips (quasi-planar polycarboxylate surface; Creoptix AG, Switzerland). After a borate buffer conditioning (100 mM sodium borate pH 9.0, 1 M NaCl; Xantec, Germany) strepdavidin was immobilized through a standard amine coupling protocol, followed by passivation of the surface (0.5% BSA [Roche, Switzerland] in 10 mM sodium acetate pH 5.0) and final quenching with 1 M ethanolamine pH 8.0 for 7 min (Xantec, Germany). The biotinylated $FLS2^{ECD}$ was coupled to the strepdavidin coated chip until the desired density was reached. For peptide binding experiments, the respective peptide was injected in a 1:2 dilution series in 20 mM citrate pH 5.0, 250 mM NaCl at 25°C. BAK1 binding kinetics were determined in a 1:2 dilution series, with the respective peptide present at 0.5 · K_D in all blank - and BAK1 injections. Blank injections were used for double referencing and a DMSO calibration curve was used for bulk correction. Analysis and correction were performed using the Creoptix WAVEcontrol software (applied corrections: X and Y offset, DMSO calibration, double referencing) using a one-to-one binding model.

Plant material and growth conditions

Arabidopsis thaliana accession Columbia (Col-0) was used as wild type in all experiments performed. The mutant line *fls2 efr* (SAIL_691_C4 / Salk_044334) was described elsewhere (Nekrasov et al., 2009). The transgenic lines *proFLS2:FLS2-GFP*

(Chinchilla et al., 2007), *proMYB51:NLS-3mVenus* (Poncini et al., 2017)*, proWRKY11:NLS-3mVenus* (Poncini et al., 2017), *proCYP71A12:GUS* (Millet et al., 2010), and *proBIK1:BIK1-HA* (Kadota et al., 2014) were described previously. Plants were grown on soil in short-day light conditions (12 h light/12 h dark) or vertically in Petri dishes containing 1/2 Murashige and Skoog (MS) medium (Duchefa), 0.8% plant agar (ITW reagents), and 1% sucrose in long-day light conditions (16 h light/8 h dark).

MAMP responses assays

ROS bursts and seedling growth inhibition (SGI) assays were performed as previously described (Lozano-Durán and Belkhadir, 2017). Briefly, for ROS burst assays, leaf discs (diameter 5 mm) were cut out from 6-week-old healthy Col-0 or *fls2 efr* plants (at least 12 discs per peptide tested). The discs were placed in a 96-well plate (Griner Bio one, Cat. No. 675 074) containing 100 μl sterile MonoQ water, with the adaxial side up. Discs were vacuum infiltrated for 10 min and incubated for 5 h in continuous light at 21°C. Alternatively, when using Sigma-Aldrich luminol at a concentration 0.034 mg/ml (see below), the discs were left in the dark for 16 h, (Figure S4F). Next, the water was carefully removed and replaced with 100 μl of elicitation solution containing Horse Radish Peroxidase (ThermoFisher Scientific) at a final concentration of 0.04 mg/ml or 0.02 mg/ml, L-012 at a final concentration of 0.068 mg/ml (Wako Chemicals) or luminol at a final concentration of 0.034 mg/ml (Sigma-Aldrich), and flg22 peptide at concentrations ranging from 10 nM to 10 μM. Immediately afterwards, the measurement of relative luminescence was started using a BiTec Synergy 4 microplate reader. The luminescence was measured every minute for 40 min and the total relative light units for the 40 time points were used for the analysis. For the measurement of SGI, Col-0 or *fls2 efr* mutant plants were grown vertically on 1/2 MS plates for 5 days. Next, the seedlings were transferred to a 48-well plate (Griner Bio one, Cat. No. 677180) containing 1 ml of liquid MS medium supplemented with flg22 peptides at a concentration of 10 nM. The fresh weight of each seedling was measured 9 days later. Each experiment included the mock control and seedlings treated with flg20 as a negative control. At least 8 seedlings per treatment were measured. The inhibition of seedling growth was calculated for each flg22 peptide compared to the median fresh weight of the mock control.

Plant bacterial assays

Arabidopsis infection assays with *Pseudomonas syringae pv. tomato* DC3000 ΔfliC - EV, -FliC Pa flg22 and -FliC Pa flg22^{Q20D} were performed as previously described (Zipfel et al., 2004) with some modifications. Bacterial growth in plant leaves was assessed by spraying 4-week-old WT and *fls2 efr* (Nekrasov et al., 2009) plants with a bacterial inoculum of OD600 = 0.2 in 10 mM MgCl2 supplemented with 0.02 % Silwet L-77. Three days after inoculation each sample (8 leaf discs from 4 different plants) were bored from the sprayed areas and homogenized in 10 mM MgCl2. The bacterial titer was determined by plating and serial dilution. Leaf pictures and disease symptoms scores were acquired five days after inoculation.

Imaging of fluorescent transcriptional reporter lines

5-day-old seedlings grown on 1/2 MS plates were transferred to liquid medium supplemented with the different flg22 peptides at 10 nM. After 24 hr, confocal laser scanning microscopy experiments were performed using a Zeiss LSM780 microscope. Excitation and detection windows were set at 488 nm and 493-598 nm respectively. The adaxial side of the leaves for *proWRKY11:NLS-3mVenus* and root tip for *proMYB51:NLS-3mVenus* were imaged. Confocal images were processed and analyzed using Fiji (Schindelin et al., 2012).

Imaging of the CYP71A12 beta-glucuronidase transcriptional reporter system

5-8 *proCYP71A12:GUS* seedlings were germinated in a 48-well plate (Griner Bio one, Cat. No. 677180) in 1/2 MS liquid supplemented with 0.5 g/l MES (Millet et al., 2010). After 7 days, a solution of antagonist peptide at a final concentration 100 μM was added and pre-incubated with seedlings for 15 min. Next, the media was supplemented with 10 nM Pa flg22 and incubated 5 h at 21°C. The media was then removed, and each well was washed with 50 mM sodium phosphate (pH 7). The GUS substrate solution was added (50 mM Na$_3$PO$_4$, 10 mM EDTA, 0.5 mM K$_4$[Fe(CN)$_6$], 0.5 mM K$_3$[Fe(CN)$_6$], 0.5 mM X-Gluc, 0.01 % Silwet L-77) and incubated overnight in the dark at 37°C. Seedlings were then fixed in 3:1 EtOH:acetic acid at 4°C for 5 h and stored in 95% EtOH. Root pictures were taken using a Leica M205FA stereoscope coupled to a Leica DFC310FX camera.

FLS2-BAK1 interaction using an enzyme-linked immunosorbent assay

Ectodomain interaction studies were performed as previously described (Smakowska-Luzan et al., 2018) with minor modifications. FLS2^{ECD} cloned in pECIA2 (bait protein) and BAK1^{ECD} cloned in pECIA14 vector (prey protein) were expressed via transient transfection in *Drosophila melanogaster* Schneider 2 (S2) cells with Expres2 TR Transfection Reagent (Expression System). Upon transfection, the cells were shifted from 27°C to 21°C. 24 h later, protein expression was induced with 1 mM CuSO$_4$. Supernatant was collected three days after induction and protein expression was confirmed by immunoblotting using anti-V5-HRP (Invitrogen, Cat. No. R961-25) and anti-Flag-HRP (Sigma Aldrich, Cat. No. A8592) antibodies to detect the bait and prey proteins respectively. FLS2^{ECD} and BAK1^{ECD} were diluted in 1x PBS containing 0.1 % Tween-20 (PBS-T) and mixed 1:1. flg22 peptide was added to mix to a final concentration ranging from 10 nM – 1 μM, depending on the assay. The protein mix was pre-incubated 2 h at 4°C. 100 μl of the protein solution was then transferred to a protein-A coated 96 well plate (Sigma Aldrich, Cat. No. 15132) and incubated overnight at 4°C. The next day, the plate was washed two times with 100 μl PBS-T and 100 μl of KPL BluePhos alkaline phosphatase was added (Sera care, Cat. No. 5120-0059). 2 h after addition of the substrate, absorbance was measured at 650 nm using a Synergy

H4 Multi-Mode plate reader (BioTek). Each plate contained a BIR4-BAK1 positive control (Smakowska-Luzan et al., 2018). To control for unspecific binding of prey protein to protein A coated wells, the bait protein was substituted with a solution of human recombinant IgG1-Fc protein (Invitrogen, Cat. No. 13445946) at a final concentration of 625 pg/μl. For each flg22 peptide tested, relative A650 was quantified by dividing the raw A650 after 2 h to the signal of the mock control.

Protein extraction and co-immunoprecipitation in Arabidopsis

0.8 g of 2-week-old seedlings of *proFLS2:FLS2-GFP* or Col-0 grown vertically on 1/2 MS plates were placed in a 6-well plate (Griner Bio one, Cat. No. 657185) and rinsed with 5 ml of sterile water. Next, the water was exchanged for either elicitor solution at final concentration of 100 nM, or with 10 nM Pa flg22 and increasing concentrations of antagonistic flg22 peptide. The seedlings were vacuum infiltered for 10 min and immediately afterwards ground in liquid nitrogen to obtain a fine powder. 2-3 ml of extraction buffer (50 mM HEPES pH 7.5, 100 mM NaCl, 10 mM MgCl2, 10% glycerol, 2 mM EDTA, 1 mM Na_2MoO_4, 20 mM NaF, 1 mM DTT, EDTA-free protease inhibitor cocktail (Roche), 1% IGEPAL) was added to each sample. The tissue was additionally homogenized with a Polytron (Kinematica) and incubated for 30 min at 4°C. The samples were then centrifuged for 10 min, 4°C, 13000 rpm and the supernatant were filtered through Miracloth (Merck Millipore Calbiochem, Cat. No. 475855-1). Next, the supernatant was diluted 1:1 in extraction buffer without IGEPAL, and 15 μl of equilibrated GFP-Trap A beads (Chromotek, Cat. No. gta-100) were added to each sample. The samples were incubated for 4 h at 4°C with rotation (12 rpm) and washed 4 times with 1 ml of washing buffer (50 mM HEPES pH 7.5, 100 mM NaCl,10 mM MgCl2, 0.1% IGEPAL). The protein complexes were eluted with Laemmli sample buffer (2x), boiled for 10 min at 95°C and analyzed by SDS-PAGE followed by immunoblotting using anti-GFP-HRP (Sigma) or anti-BAK1 antibodies (Agrisera, Cat. No. AS12 1858) with anti-Rabbit-HRP antibodies (Sigma Aldrich, Cat. No. A6154).

BIK1 phosphorylation assay

Four 2-week-old *proBIK1:BIK1-HA* seedlings (Kadota et al., 2014), grown on ½ MS plates, were transferred to a 6-well plate (Griner Bio one, Cat. No. 657185) and rinsed with sterile water. Next, the water was replaced by a solution containing flg22 at a final concentration of 100 nM. The seedlings were vacuum infiltrated for 10 min. Immediately afterwards, the seedlings were transferred to 2 ml tubes containing glass beads and 300 μL of protein extraction buffer (50 mM TRIS pH 7.5, 100 mM NaCl, 10 % glycerol, 5 mM EDTA, 1 mM Na_2MoO_4, 20 mM NaF, 1 mM DTT, EDTA-free protease inhibitor cocktail (Roche, Cat. No. 45-5056489001)). The samples were ground with a Precellys homogenizer (2 x 40 sec; 4800 rpm). After centrifugation (10 min, 13000 rpm, 4°C), the supernatant was boiled for 10 min at 95°C with Laemmli sample buffer. Analysis of BIK1 phosphorylation was performed by SDS-PAGE followed by immunoblotting using anti-HA-HRP (Sigma Aldrich, Cat. No. A8592) antibodies.

Flg22 phylogenetic tree

Molecular phylogenetic analysis of flg22 sequences was done by using the Maximum Likelihood method based of the Whelan And Goldman model (Whelan and Goldman, 2001). The tree with the highest log likelihood (-553.20) is shown. Initial tree(s) for the heuristic search were obtained automatically by applying Neighbor-Join and BioNJ algorithms to a matrix of pairwise distances estimated using a JTT model, and then selecting the topology with superior log likelihood value. The tree is drawn to scale, with branch lengths measured in the number of substitutions per site. The analysis involved 48 amino acid sequences. A total of 22 positions are included in the final dataset. Evolutionary analyses were conducted in MEGA7 (Kumar et al., 2016).

Analysis of co-mutation sites in FliC

Mutual Information Theory (MIT) was used to identify residues in FliC proteins that are coevolving in *Pseudomonas* (Gouveia-Oliveira and Pedersen, 2007). Two datasets, 528 complete genomes from the online Pseudomonas Database (Winsor et al., 2016) and 1490 genomes (Karasov et al., 2018) were downloaded and FliC proteins were identified as described in (Colaianni et al., 2021). We then used muscle to align the FliC proteins, and trimal to remove columns with gaps in 10% or more of the sequences for each dataset separately (Capella-Gutiérrez et al., 2009; Edgar, 2004). We calculated the Mutual Information (MI) and performed row-column weighting (RCW) as described in (Gouveia-Oliveira and Pedersen, 2007). Briefly, MI was calculated with the equation:

$$MI(A;B) = \sum_i \sum_j P(a_i, b_j)\log\left[\frac{P(a_i, b_j)}{P(a_i)P(b_j)}\right]$$

A and *B* are the sites being compared, and *i* and *j* run through all of the amino acids at the site. The estimation of the probabilities was performed by using the observed frequencies found in the dataset. After calculating MI at each site, we performed RCW to adjust the MI for sites that are rapidly evolving. This increases the chances of identifying true co-evolving sites. We used the formula in (Gouveia-Oliveira and Pedersen, 2007)

$$RCW(A;B) = \frac{MI_{ij}}{\frac{MI_j + MI_{i.} + MI_{j.} + MI_{i.} - 2MI_{ij}}{2n-2}}$$

Where MI_j denotes the sum of the Mutual Information matrix over all lines in column *j*. These adjusted MI values were then used to calculate Z-scores for each value. We considered the residue pairs with MI values in the top 0.5% as co-evolving sites. The codes and raw data for MIT is available at https://github.com/ncolaian/flagellin_antag_pleiotropy.

Identification of non-synonymous SNPs in natural accessions of Arabidopsis

To parse the non-synonymous single nucleotide polymorphisms (SNPs) in *FLS2* and *BAK1* from the genomes of 1135 naturally inbred lines of *Arabidopsis thaliana*(1001 Genomes Consortium, 2016b), we build an in-house snprator.r script in the R programming environment. The script and necessary genomic data are freely accessible under the link: https://github.com/arthurkorte/SNP_extractor. As an output, a list of identified SNPs, the chromosomal positions, frequency of the SNPs, and accession ID numbers that carry the SNP are retrieved (Table S6).

QUANTIFICATION AND STATISTICAL ANALYSIS

Programs used for statistical analysis and data visualization

GraphPad PRISM 8.0 and R programming environment (version R 3.6.0) were used for data analysis and visualization. In all assays performed, data were combined from at least two independent biological experiments. Unless specified otherwise, the box plot represents the first and third quartiles, centered by the median. Whiskers include the 10th-90th percentile of the data points. Dots represent individual observations. Outliers were removed using the ROUT test, implemented in GraphPad PRISM (Q = 0.1%). Non-mutated Pa flg22 peptide was used as a control sample and comparator in all statistical tests performed, except in Figures 5D and 5E where pairwise comparison was performed. Unless otherwise indicated, the calculated p values indicate the likelihood that the tested variant differs significantly from Pa flg22 at a 95% confidence level. One-way ANOVA followed by Dunnett's or Sidak multiple comparisons test was performed using GraphPad PRISM 8.0 and one-way ANOVA followed Tukey's multiple comparisons test was performed using R. The ROS burst and SGI results were analyzed using a mixed effect linear model as previously described (Smakowska-Luzan et al., 2018). Briefly, the statistical analyses were performed in R version 3.6.0. The lme4 package was used for model construction. In this model, the non-mutated flg22 was used as a fixed effect and each experiment performed as a random effect using the formula ROS ~ Variant + (1 | Trial) and SGI ~ Variant + (1 | Trial), respectively. Subsequently, the lmerTest package was implemented to calculate p values using Satterthwaite approximation and the resulting p values were corrected for multiple testing using the Holm method. To determine if peptides produced significant ROS and SGI phenotypes (Figure S4C), we compared the 95% confidence intervals for the mean of each peptide's measurements to the 95% confidence intervals for the mean in 10000 independent samples with equal n from the Pa flg20 measurements. A significant difference was designated when the confidence intervals did not overlap in >95% of the samples. To estimate the relationship between bacterial motility and FLS2 binding within different categories designated based on the binding affinities, Kolmogorov-Smirnov test in R programming environment was used (R version 3.6.0). Flagellin structure was modeled using PyMOL software (PyMOL v1.6.0.0) and flg22 amino acid sequence LOGOs were generated using WebLOGO portal (Crooks et al., 2004). The plots presented in Figures 1B and 3A were generated using RainCloud (Allen et al., 2019).